

# Submillimetre point sources from the Archeops experiment: Very Cold Clumps in the Galactic Plane

F.-X. Désert<sup>1</sup>, J. F. Macías-Pérez<sup>2</sup>, F. Mayet<sup>2</sup>, G. Giardino<sup>7</sup>, C. Renault<sup>2</sup>, J. Aumont<sup>2</sup>, A. Benoît<sup>3</sup>, J.-Ph. Bernard<sup>4</sup>, N. Ponthieu<sup>5</sup>, and M. Tristram<sup>6</sup>

<sup>1</sup> Laboratoire d’Astrophysique, Obs. de Grenoble, BP 53, 38041 Grenoble Cedex 9, France

<sup>2</sup> LPSC, Université Joseph Fourier Grenoble 1, CNRS/IN2P3, Institut National Polytechnique de Grenoble, 53 avenue des Martyrs, 38026 Grenoble cedex, France

<sup>3</sup> Centre de Recherche sur les Très Basses Températures, BP166, 38042 Grenoble Cedex 9, France

<sup>4</sup> Centre d’Étude Spatiale des Rayonnements, BP 4346, 31028 Toulouse Cedex 4, France

<sup>5</sup> Institut d’Astrophysique Spatiale, Bât. 121, Université Paris XI, 91405 Orsay Cedex, France

<sup>6</sup> Laboratoire de l’Accélérateur Linéaire, BP 34, Campus Orsay, 91898 Orsay Cedex, France

<sup>7</sup> ESA - Research and Science Support Department, ESTEC, Postbus 299, 2200 AG Noordwijk The Netherlands

October 27, 2018

## ABSTRACT

**Aims.** Archeops is a balloon-borne experiment, mainly designed to measure the Cosmic Microwave Background (CMB) temperature anisotropies at high angular resolution ( $\sim 12$  arcminutes). By-products of the mission are shallow sensitivity maps over a large fraction of the sky (about 30 %) in the millimetre and submillimetre range at 143, 217, 353 and 545 GHz. From these maps, we produce a catalog of bright submillimetre point sources.

**Methods.** We present in this paper the processing and analysis of the Archeops point sources. Redundancy across detectors is the key factor allowing us to distinguish glitches from genuine point sources in the 20 independent maps.

**Results.** We look at the properties of the most reliable point sources, totalling 304. Fluxes range from 1 to 10,000 Jy (at the frequencies covering 143 to 545 GHz). All sources are either planets (2) or of galactic origin. The longitude range is from 75 to 198 degrees. Some of the sources are associated with the well-known Lynds Nebulae and HII compact regions in the galactic plane. A large fraction of the sources have an IRAS counterpart. Except for Jupiter, Saturn, the Crab and Cas A, all sources show a dust-emission-like modified blackbody emission spectrum. Temperatures cover a range from 7 to 27 K. For the coldest sources ( $T < 10$  K), a steep  $\nu^\beta$  emissivity law is found with a surprising  $\beta \sim 3$  to 4. An inverse relationship between  $T$  and  $\beta$  is observed. The number density of sources at 353 GHz with flux brighter than 100 Jy is of the order of 1 per degree of Galactic longitude. These sources will provide a strong check for the calibration of the Planck HFI focal plane geometry as a complement to planets. These very cold sources observed by Archeops should be prime targets for mapping observations by the Akari and Herschel space missions and ground-based observatories.

**Key words.** ISM: general – ISM: clouds – Methods: data analysis – Cosmology: observations – Submillimeter – Catalogs

## 1. Introduction

ARCHEOPS is a balloon-borne experiment following on from the PLANCK satellite and its High Frequency Instrument (HFI). It measures the Cosmic Microwave Background (CMB) temperature anisotropies at high angular resolution ( $\sim 12$  arcminutes) over a large fraction of the sky (around 30 %) in the millimetre and submillimetre range at 143, 217, 353 and 545 GHz. The main results of cosmological nature have been discussed elsewhere (Benoît et al. (2003a), Benoît et al. (2003b), Tristram et al. (2005)). But because we have, for the first time, a large survey of the millimetre sky, studies on other scientific topics can be performed. Detection of large-scale polarized dust emission is reported in Benoît et al. (2004), Ponthieu et al. (2005). The large scale spectral properties of the dust emission have been investigated by Bernard (2004) and finally, the statistical detection of clusters of galaxies is shown by Hernández-Monteagudo et al. (2005).

Here, we analyze another by-product of the ARCHEOPS mission. We look at the properties of the most reliable point sources

in the ARCHEOPS survey. We discuss the extraction method, the catalog of candidate cold dust clumps of likely galactic origin, as well as two planets and two supernova remnants. Some of these clumps are producing massive stars. Implications for the galactic clump mass distribution function and the expected number of Galactic point sources in the PLANCK survey are then discussed.

## 2. Point-source extraction

### 2.1. The instrument

The gondola contains a primary mirror with an effective 1.5 m diameter, a secondary mirror and a photometer containing spider-web bolometers cooled to 100 mK. The instrument is described in detail by Benoît et al. (2002) and Macías-Pérez et al. (2007). The ARCHEOPS 353 GHz channel consists of three pairs of bolometers mounted on polarizer dichroics so as to detect the polarized diffuse emission of Galactic dust. The telescope boresight angle is 48 deg. with respect to the zenith. The gondola is made spins at 2 rpm via a motor fixed on the balloon chain. The Eastward balloon trajectory and the Earth rotation make the instantaneous circle drift

on the celestial sphere. This scanning strategy produces a shallow survey of a large fraction of the sky in few hours. The angular resolution varies from 15 to 8 arcminutes (FWHM) with the channel frequency from 143 to 545 GHz. The sensitivities and main data processing methods are described by Macías-Pérez et al. (2007). We use the data from 6 detectors at 143 GHz, 7 at 217 GHz, 6 at 353 GHz and one at 545 GHz.

## 2.2. The method

Because of the scanning strategy, one detector will sweep rapidly a given diffraction spot of the sky. Instead of using the timeline signature of point sources (impulse convolved with beam response) which can be confused with glitches (impulse only), we prefer to use the redundancy between the 20 available bolometers at the map level. Glitches will fall at random locations, whereas point sources will produce a concentration of bright spots in the same sky position in several bolometer maps. The detection process is a separate step from the measurement process. Once a candidate location is found, the point-source flux and error are measured on all bolometer maps and coadded with natural weights.

The data from the last flight (KS3, 2002, Feb. 7th) only are used, with a time range between 15.4 and 27.3 UT (well within night time). What is projected on sky maps is between 15.5 and 27 UT.

## 2.3. Timeline processing

The Galactic timeline processing is described by Macías-Pérez et al. (2007) and is slightly different from the CMB one. An example is shown in Fig. 1. The low frequency thermal drifts, the atmospheric emission and the Galactic diffuse emission signal produce a varying background signal. Stripes can be produced that degrade the efficiency of point-source detection. Therefore, it is necessary to subtract the baseline. The timeline, which is masked and interpolated around glitches or strong point sources, is smoothed in order to provide this baseline, to be subtracted from the initial time ordered information (hereafter TOI). The smoothing occurs, first over a period of several revolutions, then over lengths of ninety degrees on the instantaneous circle described by the gondola. Atmospheric noise can leave residues on ten degree scales. A timeline component separation is done on these scales or larger. The clean timeline (CToi) is ready for map making. We also produce a clean deglitched timeline (CDToi) to be used for faint point source and background map computations.

## 2.4. Map-making

The prepared timelines have white noise properties. Thus we proceed with a simple map-making with a natural weighting of the prepared timelines (CToi and CDToi) for each detector, using pointing information from the star sensor and the known detector position in the focal plane. The map is made in the Healpix scheme (Gorski et al. (2005)) with  $N_{\text{side}} = 512$ . It provides a 7-arcmin pixel size which is adequate to sample the point-spread-function. The map is smoothed with a 12-arcminute circular Gaussian kernel in order to prepare for the point-source detection processing. A background component is evident with angular scales of a few degrees, due to the Galaxy diffuse component emission (mostly due to interstellar dust at these frequencies). We compute a smooth background component (Fig. 2)

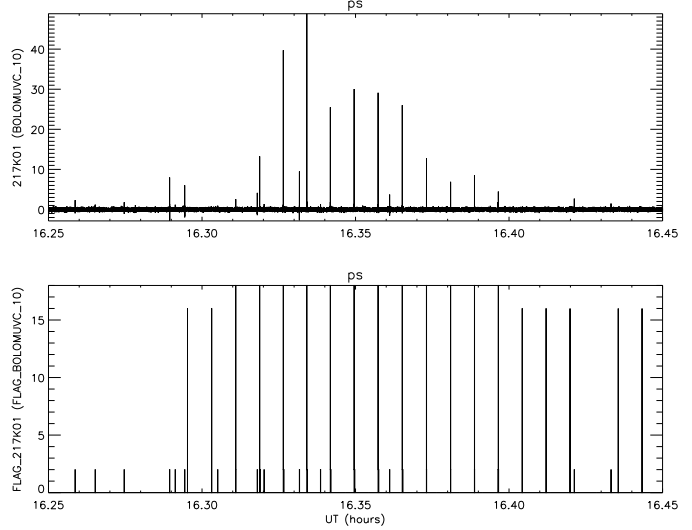


**Fig. 1.** Extract of the bolometer 217K01 signal timeline (upper plot). Note the regular spikes produced by Jupiter, when the gondola crosses its line of sight at each revolution (pendulation explains why the spike intensity is not smooth during the different crossings). On the other hand, cosmic ray hits happen at random times. The lower plot indicates the cumulated flagging found during data processing (a value of 2 for glitches and a value of 16 around known point sources).

by projecting the CDToi and then smoothing the resulting map with a 60 arcminute circular Gaussian kernel. The smoothing is done in the spherical harmonic space. Pixels that were unobserved (at the edge of the survey) are replaced by zero before the spherical harmonic transform is done. The final background-subtracted map is then computed for each detector. Thus, the end map represents for each bolometer the sky convolved with a 12-arcmin. Gaussian kernel minus a 60-arcmin. Gaussian kernel. This spatial filter has a zero mean and is appropriate for a simple point-source detection-by-thresholding algorithm. We also produce channel maps obtained by optimal coaddition of those previous maps for detectors of a given channel (*i.e.* at the same frequency). A relative calibration between detectors is used for that coaddition, which is described in Macías-Pérez et al. (2007).

## 2.5. Point-source extraction

Outside the galactic plane, the detector map is dominated by noise. A Gaussian function is fit to the histogram of the product of the pixel value  $v_p$  by the square root of the number of hits  $N_p$ . For a given detector, the dispersion  $\sigma_d$  gives the typical elementary noise value for one hit, *i.e.* for one data sample, the data acquisition rate being 153 Hz. It is then used to estimate the noise on each pixel as  $\sigma_p = \sigma_d / \sqrt{N_p}$ . A listing of target pixels defined as  $\frac{S}{N} = |\frac{v_p}{\sigma_p}| > 5$  is produced for each detector. At this stage glitches and point sources are not separated. Two catalogs are obtained depending on whether one uses the CToi (still containing hits from strong point sources and glitches) or the CDToi (having strong point sources and glitches removed). For the CToi catalog, we perform a final separation of point sources from glitches by requesting that, for a point-source, the above 5  $\sigma$  detection criteria for a given sky pixel be matched by at least 5 different detectors. For the CDToi catalog, we use the final

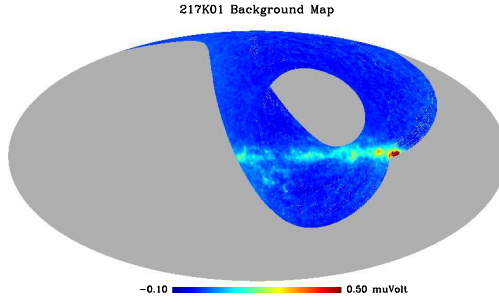


**Fig. 2.** Background map of the 217K01 detector. This map is obtained by projecting the clean deglitched timeline and by smoothing the result with a 60 arcmin. circular Gaussian kernel. An all-sky Mollweide projection, with the Galactic Anticenter at the center of the projection, is used throughout this paper. About 30 percent of the sky was observed. This smooth map is subtracted from the detector map in order to find the point sources by a simple thresholding algorithm.

point-source criterium that at least two channel maps have  $4\sigma$  detections. A channel map is defined here as the optimal average of the maps of all detectors at the same frequency. Out of the 4500 pixels that satisfy the criteria, some are connected to each other and correspond to the same point-source. To have a single position for each point-source, we keep the pixel for which a maximum number of detectors have a  $5\sigma$  detection. This defines a final catalog of sources. For each of them, we can measure the flux, error and position on the 20 independent detector maps and the 4 channel maps.

Fig. 3 shows the flux comparison of the two methods (CToi and CDToi) for the 87 sources in common in the two catalogs. A very good agreement is obtained for most of the flux range and for all four frequencies. At the bright end, we expect and observe that the deglitching slightly biases the flux measured from the CDToi (“CD” fluxes in the abscissae of the figure). However, the CDToi method is more powerful at the faint end, because the signal to noise ratio benefits from the coaddition. We have therefore merged the two catalogs. For each of these candidates, we average the flux from different bolometers in each of the 4 frequency bands with a natural weight (equal to the inverse square of the noise). Positions are measured with the same weighting. From the internal dispersion between channel positions, we have estimated the  $1\sigma$  position accuracy to be about 4 arcmin (a third of the beam width). For 23 of the brightest point sources, one of the channel position disagrees with the final position. Nearby glitches in the CToi objects and confusion might cause such a systematic effect.

### 2.6. Flux calibration and planet observations

The flux calibration is performed at this stage. The CMB dipole calibration is used at 143 and 217 GHz and the FIRAS galactic calibration is used at 353 and 545 GHz (see details in Macías-Pérez et al. (2007)). These are extended source calibrations. In order to propagate them to point-source calibration, we integrate the beams measured on Jupiter and Saturn. Assuming angular diameters for these (unresolved) sources of 44.60 by 41.71 arcseconds and 19.05 by 17.00 arcseconds respectively, we obtain the brightness temperature given in Table 1. Statistical error bars are negligible. The total error bars are made up from

an absolute calibration error (resp. 4, 8, 12, and 8 %), the estimated error due to the beam integration procedure (estimated by comparing the beam shape obtained from Jupiter and Saturn observations at the same frequency) and an intercalibration error (the measurement dispersion across the bolometers at the same frequency).

$\nu$ (GHz)	Jupiter		Saturn	
	$T_{RJ}$ (K)	$\sigma$ (K)	$T_{RJ}$ (K)	$\sigma$ (K)
143	165	20	160	19
217	139	22	144	23
353	159	24	179	27
545	146	20	166	23

**Table 1.** Jupiter and Saturn brightness temperature, as calibrated with Archeops extended source calibrators (the CMB dipole at 143 and 217 GHz and the FIRAS Galaxy at 353 and 545 GHz). Error bars are absolute calibration errors.

Figure 4 shows the (sub)millimetre spectrum of Jupiter and Saturn, as measured by WMAP (Page et al. 2003), ARCHEOPS and Goldin et al. (1997). There is a broad agreement of the flux scale over a factor of 20 in frequency range. The ratio of Jupiter to Saturn flux at a given frequency, which should be independent of the absolute flux scale calibration, is larger in ARCHEOPS than in the Goldin et al. (1997) measurements. Explanations might be sought in small non-linearity problems in the ARCHEOPS instrument for these very high flux sources and also from the simplified emission assumptions of the two planets (inclination of Saturn rings), as shown by the detailed PRONAOS calibration (Pajot et al. (2006)).

In addition to the systematic errors discussed above, for the point source catalog, we need to consider the error introduced by the flux measurement method described in Sect. 2.5. The convolution by a simplified 2D Gaussian kernel increases the measurement intrinsic dispersion of bolometers at a single frequency. For the final catalog, we estimate the absolute calibration scale uncertainties as 14, 21, 17, and 15 % at 143, 217, 353, and 545 GHz respectively.

## 3. Results

### 3.1. The point-source catalog

ARCHEOPS has detected 304 submillimetre point-sources in the covered 30.0 % fraction of the sky. These are plotted in Fig. 5. They are mostly in the Galactic Plane, with a high concentration in the Cygnus and Taurus complexes. Fluxes range from 1 to  $10^4$  Jy and median average fluxes and errors are 3.0 and 1.4 Jy at 143 GHz, 19 and 3 Jy at 217 GHz, 76 and 13 Jy at 353 GHz, and 344 and 44 Jy at 545 GHz. The survey is inhomogeneous in sensitivity because the scanning strategy and the limited observing time did not allow an equal number of pixel hits everywhere. The obtained median sensitivities are in agreement with expectations from Table 8 by Macías-Pérez et al. (2007), giving us some confidence in the processing efficiency. The average integration time spent by an ARCHEOPS detector on a 12-arcmin spot on the sky is only 0.11 second.

The catalog of sources (the 2 planets being excluded) is given in Table 3. It includes the position on the sky with galactic coordinates in degrees, fluxes in Jy, with their error bars and signal to noise ratio. Associations with the IRAS point-source and

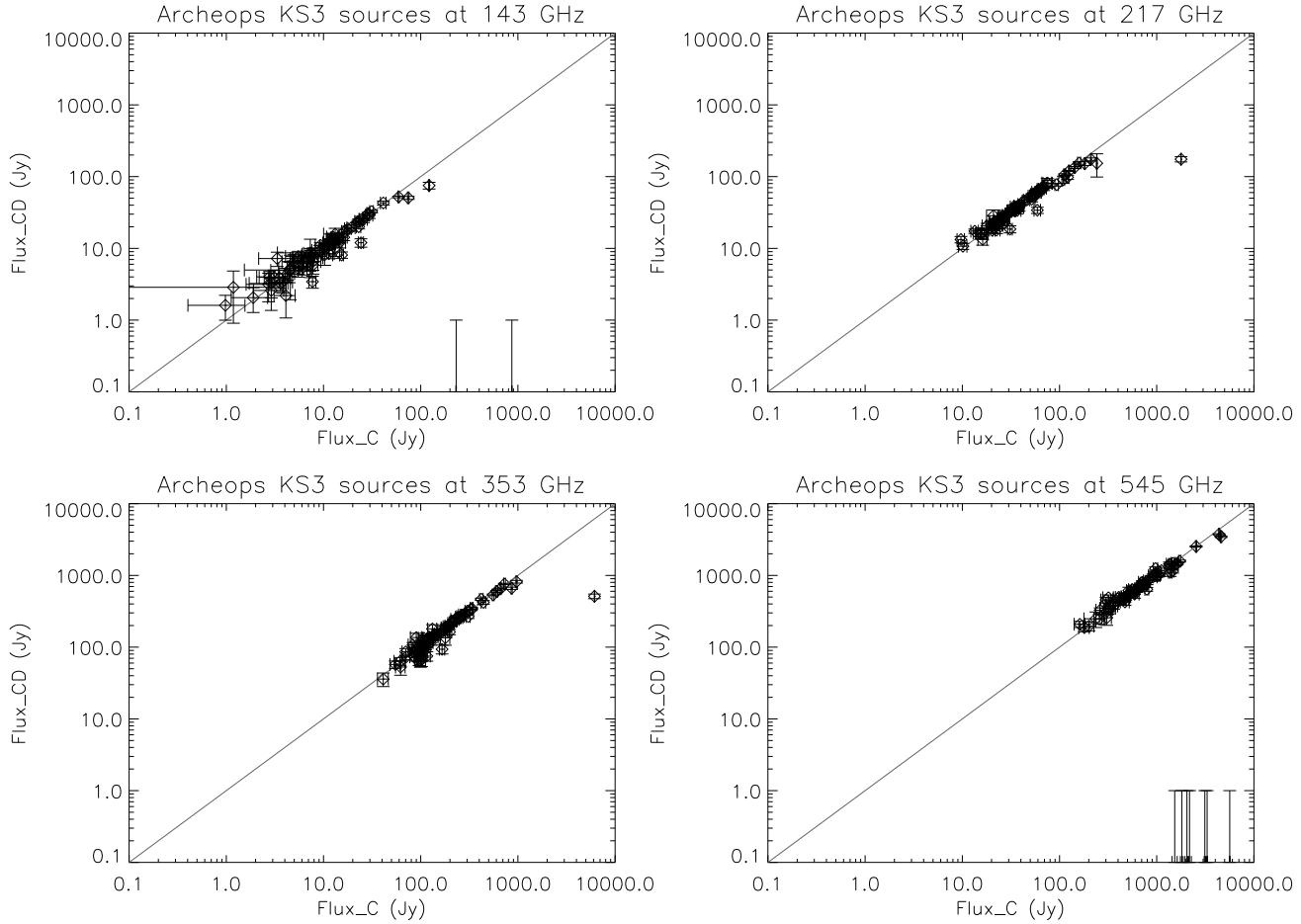


**Fig. 3.** Flux comparison between the two detection methods at the four frequencies, for sources in common to both methods. The plots compare the flux obtained with (CD) and without (C) a deglitching applied to the data.

small extended source catalog are given in Table 4. The matching radius is 10 arcmin ( $2.5\sigma$  of ARCHEOPS position accuracy). In many cases, there is more than one IRAS counterpart within the matching radius, so the source with the strongest flux at  $100\mu\text{m}$  (IRAS) was selected. Associations with previously known sources are made with CDS catalogs<sup>1</sup> (Table 4). Many sources have a counterpart with a bright or dark Lynds Nebula or an HII compact (Sharpless) region (for example, DR 21, W 3). Matches to HII regions with an angular size lower than 10 arcminutes from the catalogue of Paladini et al. (2003) are also included. Finally, in Table 4, sources whose IRAS counterpart is likely an ultra-compact HII region (UCHII) are indicated. These were identified from their IRAS color following the color criteria from Kurtz, Churchwell & Wood (1994) and applying a flux threshold of 100 Jy at  $100\mu\text{m}$  (i.e. only sources with the colors of an ultra-compact HII region and  $F(100\mu\text{m}) > 100$  Jy are indicated).

Concentration of the sources in the Galactic Plane and in molecular cloud regions indicates a galactic origin. This galactic origin of most of the sources is confirmed in Fig. 6. We compute the background expected from IRAS extrapolations (Finkbeiner et al (1999)) at the same frequency as the ARCHEOPS sources. There is not a direct correlation between the ARCHEOPS flux at 353 GHz and the diffuse background emission expected

at the same frequency, but we find in Fig. 6 that the sources tend to gather in high background regions. For example, 60 % of the point sources are in regions with an average brightness larger than  $5\text{ MJy/sr}$  at 353 GHz. Similarly, using the large scale Galactic CO survey by Dame et al. (2001), we do not find a direct correlation between the CO velocity-integrated brightness and the ARCHEOPS flux but there is a strong trend for the submillimetre sources to lie in high CO background regions. For example, half the point sources lie on top of a CO background greater than  $15\text{ K.km.s}^{-1}$  whereas half of the pixels recorded by ARCHEOPS with a CO measurement have a CO flux greater than only  $2.5\text{ K.km.s}^{-1}$

### 3.2. Photometry

We have compared the fluxes measured with ARCHEOPS with previous surveys conducted in the submillimetre domain.

In particular the Crab and Cas A point-sources are well-known sources and can be used for comparison. No other supernova remnant (Green 2004) could be associated with the present catalog.

Concerning the Cas A supernova remnant, ARCHEOPS confirms the submillimetre emission (Table 2) in excess of the synchrotron component and discovered and mapped by SCUBA (Dunne et al. (2003)). The 143 GHz point closely fits the synchrotron extrapolation (giving some confidence in the ARCHEOPS

<sup>1</sup> <http://cdsweb.u-strasbg.fr>

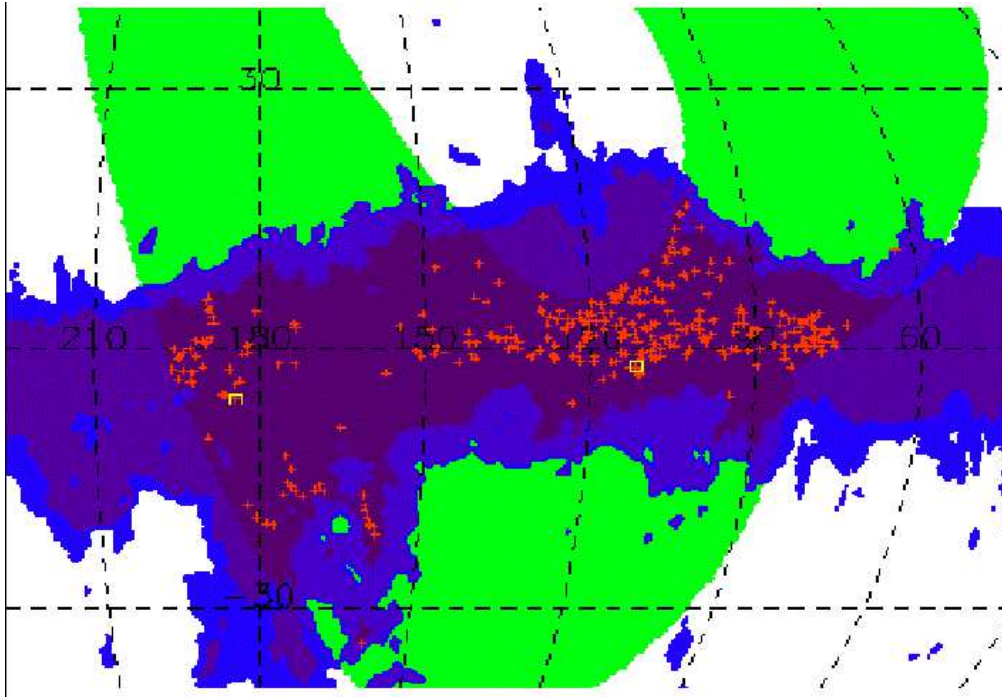


**Fig. 5.** Location of the point sources (in red pluses) in galactic coordinates in a Mollweide projection. The Crab (Tau A) and Cas A correspond to the yellow squares (from left to right). Most of the sources are concentrated in the Galactic plane. The ARCHEOPS survey is shown as the green area. A thresholded IRAS galactic map (blue) aids to trace high far-infrared background regions.

photometric calibration), whereas a large excess exists at 217, 353, and 545 GHz. The origin of this excess (cold dust, iron needles) has been debated by Dwek (2004) and Gomez et al. (2005) and is studied by Macías-Pérez et al. (2008b).

The Crab photometry is further analyzed in a companion paper (Macías-Pérez et al. (2008a)). The 143 GHz measurement is in agreement with the expected radio synchrotron component described by a power law with a spectral index  $\beta \simeq -0.299 \pm 0.009$  (Baars et al. (1977)).

Cas A		Crab	
$\nu$ (GHz)	F (Jy)	$\sigma$ (Jy)	F (Jy)
143	74.5	1.3	231.4
217	58.3	2.9	181.9
353	121	14	185
545	359	36	236

**Table 2.** Submillimetre fluxes and the statistical flux errors of the two supernova remnants detected by ARCHEOPS.

There is not a single common source with the WMAP catalog (Hinshaw et al 2007), because the WMAP catalog contains only extragalactic radio sources.

Sources observed by large ground-based telescopes are much fainter than detected as a point-source by the ARCHEOPS balloon experiment. We find that ARCHEOPS fluxes are usually greater than some of the ground-based measurements on integrated mapped regions. However, most of the present sources have never been measured at these frequencies and spatial resolution before. We can compare the flux values with the few available values ( $\sim 10$ ) published by Chini et al. (1984), Chini et al. (1986a), Chini et al. (1986b), and measured with a

90 arcsecond beam ground-based photometer at 230 GHz. ARCHEOPS values are always above the ground-based observations by a factor that can reach 10. We think that the photometric disagreement is due to the chopping techniques used in ground-based experiments and to the spatial extent of the sources.

No extragalactic point-source can be identified<sup>2</sup> in the present catalog. The strongest known extragalactic point source (for a 12-arcmin beam) is M 82 which has a flux of about 5 Jy at 353 GHz. It is not in our survey coverage, and photometrically, it is below our sensitivity limit.

### 3.3. Submillimetre spectra

Beside the 4 brightest sources (two planets and two SN remnants) most of the sources have a steep spectrum rising in the submillimetre domain with frequency, with typically an increase in flux by a factor of 100 when going from 143 GHz to 545 GHz. That excludes synchrotron or free-free emission as the main emission mechanism. Interstellar dust is most likely the source of such spectra.

Figs. 7 and 8 show the millimetre and infrared spectrum of a sample of the ARCHEOPS sources along with the IRAS measurements.

We have fitted these spectra with a simple modified black-body law:

$$F_\nu \propto \nu^\beta B_\nu(T), \quad (1)$$

with a single dust component at a temperature  $T$  and an emissivity index of  $\beta$ . The IRAS flux at 100  $\mu\text{m}$  mostly determines

<sup>2</sup> We measured the Andromeda (M 31) extended source flux within IRAS 100  $\mu\text{m}$  contour of 5 MJy/sr (about one degree size), and found a marginal detection ( $3\sigma$ ) at 545 GHz only: Fluxes of M31 : 4407 Jy at IRAS 100  $\mu\text{m}$ , < 26 Jy at 143 GHz, < 90 Jy at 217 GHz, < 340 Jy at 353 GHz and  $660 \pm 200$  Jy at 545 GHz. Upper limits are quoted as  $2\sigma$ .

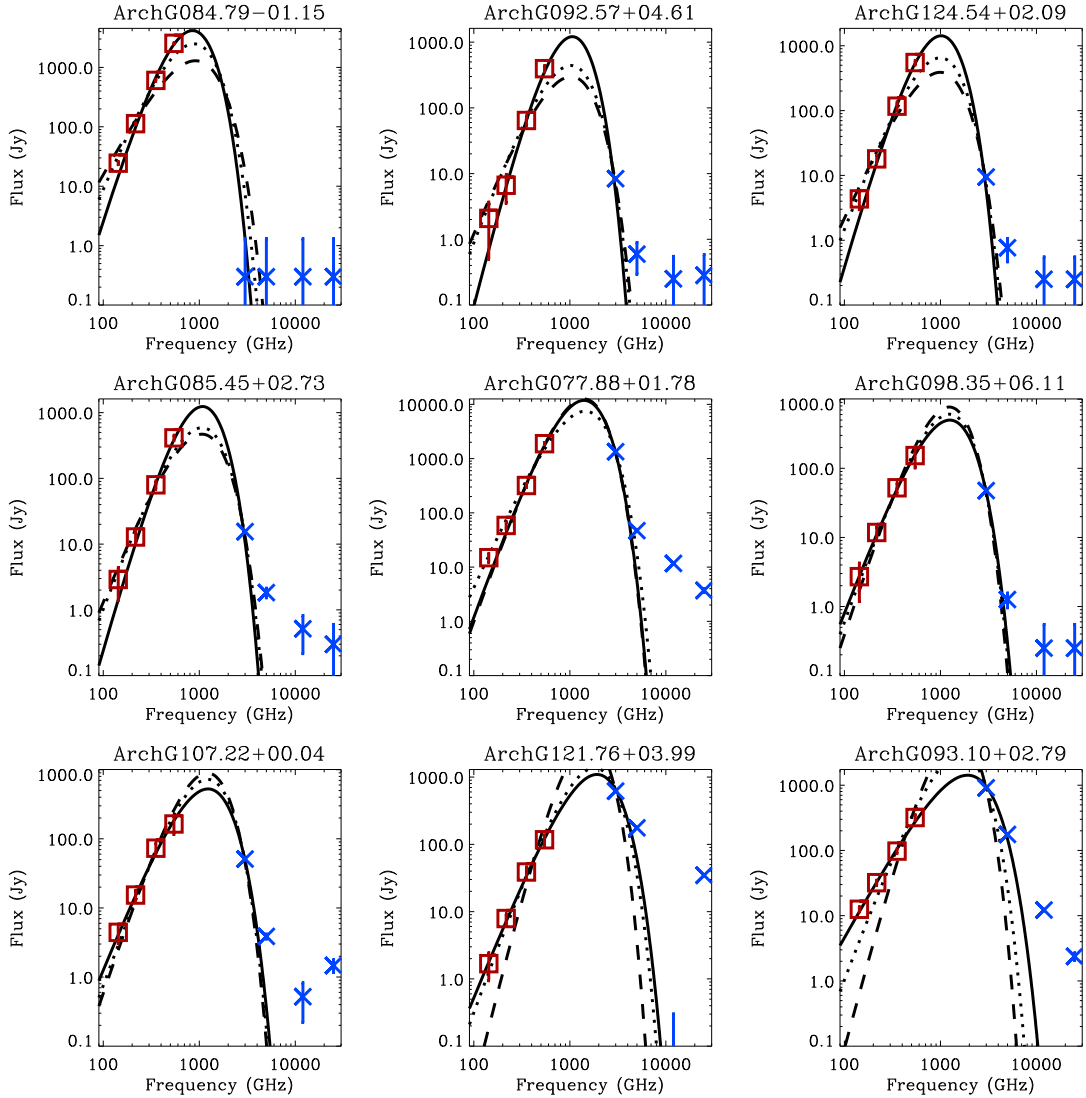


**Fig. 7.** Examples of millimetre and far infrared spectra of ARCHEOPS sources. ARCHEOPS measurements are shown with error bars as the red squares. IRAS measurements (from the point-source catalog or the small extended source catalog if present, Beichman et al. (1988)) are noted as blue crosses with their error bars. A modified blackbody law fit to the ARCHEOPS and the  $100\ \mu\text{m}$  IRAS flux is shown as a solid line. The dotted curve is obtained by fixing the emissivity exponent at a value of 2. The dashed curve is obtained by fixing the temperature at 11 K. Note the steepness of the spectrum of very cold sources in the three upper plots (sources ArchG084.79–01.15, ArchG092.57+04.61, ArchG124.54+02.09) with respect to the last lower plot on the right (source ArchG093.10+02.79).

the temperature, whereas ARCHEOPS data points lead the fit of the emissivity exponent. It is clear that the peak emission of these sources happens at the THz frequency and will have to await HERSCHEL and PLANCK observations.

The emissivity law exponent  $\beta$  and the temperature  $T$  quoted in Table 4 are found by fitting the four ARCHEOPS fluxes and the  $100\ \mu\text{m}$  IRAS flux. The fit is generally good except for 15% of the sources where the 353 GHz flux shows a small systematic deficit, or when IRAS or some ARCHEOPS band measurements are missing. The goodness of the fits has been tested using a  $\chi^2$  (quoted in Table 4) goodness-of-fit criteria at the  $2\sigma$  level. In Table 4 when the fit is unsatisfactory, we quote the emissivity index  $\beta_{11}$  obtained by fixing the temperature to 11 K in the fitting procedure, as well as the temperature  $T_2$  obtained by fixing the emissivity exponent  $\beta$  at the fiducial value of 2 (only statisti-

cal error bars are quoted). In the following we will only consider the global two-parameter ( $\beta$  and  $T$ ) fit unless otherwise stated. The fiducial temperature of 11 K was chosen as close to an average of the temperatures found in the two-parameter fits (see also Fig. 10).

### 3.4. Submillimetre point-source number counts

Excluding the four brightest sources (Jupiter, Saturn, Crab and Cas A), the study of the submillimetre spectrum of the ARCHEOPS sources indicates that they may constitute a homogenous set of dust-emission sources. Therefore, we can compute the number count of the Archeops sources. For this purpose, we fiducially choose the 353 GHz data. Fig. 9 represents the un-normalized number counts of the 353 GHz sources as a function of flux.

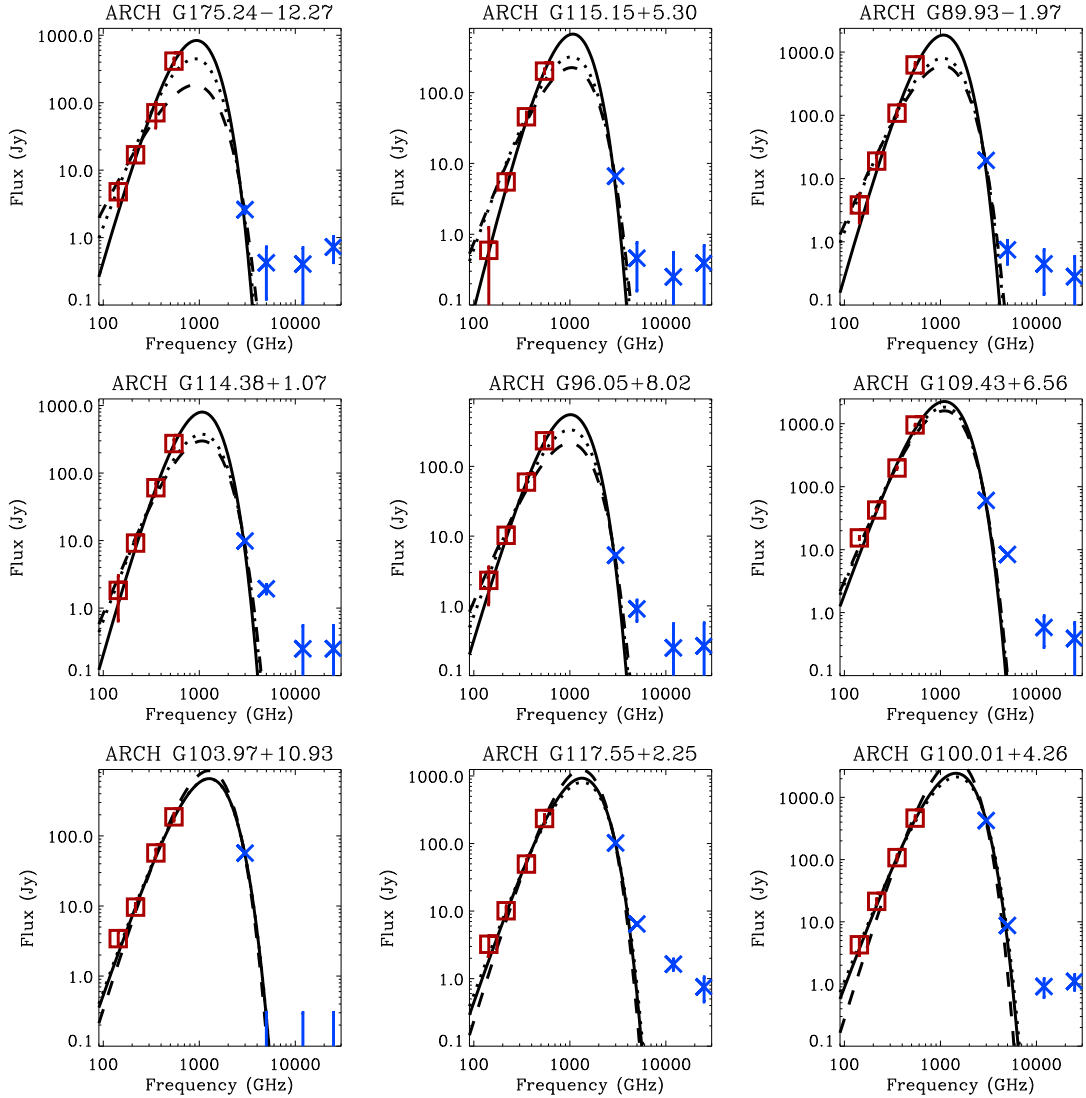


**Fig. 8.** More examples of millimetre and far infrared spectra of ARCHEOPS sources. ARCHEOPS measurements are shown with error bars as the red squares. IRAS measurements are noted as blue crosses. See Fig. 7 for explanations of the fitting lines.

We see a strong increase of the number counts with decreasing flux down to about 100 Jy, which is well above the  $4\sigma$  sensitivity level for ARCHEOPS. Then the number counts start decreasing with decreasing flux. This is mostly due to the sensitivity cut-off of Archeops at 353 GHz. At the high flux range, the number counts  $F.dN/dF$  is consistent with a power law with an exponent of  $-1.5$ .

The survey mostly covers the Galactic Plane between the galactic longitudes of 75 and 198 degrees. We can thus normalize the number counts to one degree of Galactic longitude. We obtain the following integral number counts:

$$N(> F_\nu) = (1.0 \pm 0.1 \text{ source/deg}) \left( \frac{F_\nu(353 \text{ GHz})}{100 \text{ Jy}} \right)^{-1.5 \pm 0.2}. \quad (2)$$

The number counts for the other ARCHEOPS frequencies can be computed by using a scaling factor of the form  $100 \text{ Jy} / (\nu / 353 \text{ GHz})^4$ , where  $\nu$  is the required frequency.

Assuming a constant latitude width of 10 degrees, the confusion limit, defined as one source every thirty beams, is  $\sim 27$  Jy.

This is well below the ARCHEOPS detection limit. The point-source contribution to the diffuse background is:

$$B_\nu (> F_\nu) = 0.09 \text{ MJy/sr} \left( \frac{F_\nu(353 \text{ GHz})}{100 \text{ Jy}} \right)^{-0.5}, \quad (3)$$

which is a negligible fraction of the average brightness in the Galactic Plane, unless we extrapolate the number counts to sub-Jansky levels. We can thus conclude that the galactic submillimetre sky is dominated by diffuse emission and not by point-sources.

#### 4. Discussion

Due to the limited angular resolution of ARCHEOPS, the observed point-sources are merely clumps of very cold interstellar matter. They are a sub-population of IRAS Galactic point-sources or slightly extended sources which are important for the study of the early stages of star formation. We have already noted the photometric disagreement between ground-based and the present balloon-borne measurements. Wings in shallow column

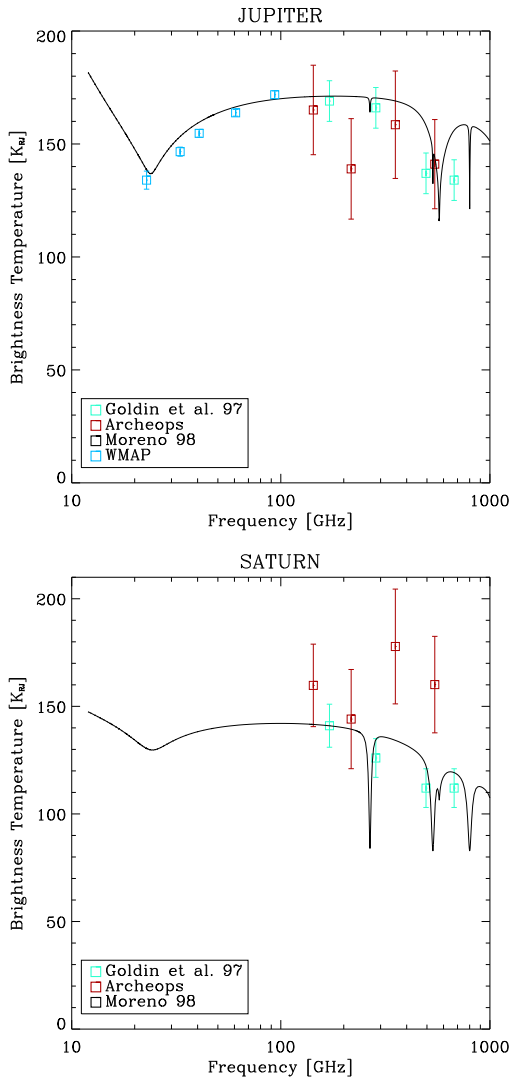


**Fig. 4.** Jupiter (upper) and Saturn (lower) flux measurements (squares) compared with Moreno's atmosphere models (lines) (Moreno (1998)) as well as WMAP and Goldin et al. (1997)'s measurements.

density profile around very dense clumps might explain the larger fluxes in ARCHEOPS photometry. Also, in order to prepare the analysis of future high frequency CMB experiments like the PLANCK satellite mission, it would be important to be able to simulate these very cold clumps in the whole sky using their spectral behavior and high frequency surveys like IRAS. We now discuss their statistical properties.

#### 4.1. Submillimetre spectral properties

In Fig. 10 we trace the emissivity law exponent  $\beta$  as a function of temperature  $T$  for the best-fit model to the spectrum of the ARCHEOPS sources. We consider only those sources for which the fit satisfies the  $\chi^2$  goodness-of-fit criteria at 95% C.L. We find that most of the sources have low temperatures ranging from 7 to 27 K. The emissivity exponent increases with decreasing temperature, going up to 4 for sources below 10 K.

The interpretation of this trend is made difficult by the intrinsic correlations between  $\beta$  and  $T$  parameters, as shown in

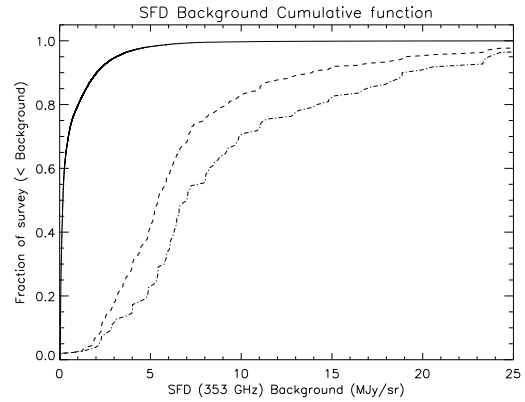


**Fig. 6.** Cumulated fraction (dashed curve) of sources falling below a given background. Here, sources are counted at the 353 GHz frequency. The background is measured as pixel value of a 353 GHz SFD map, smoothed with a 30 arcmin wide kernel. The dot-dash line shows the cumulated fraction of ARCHEOPS point sources with a flux larger than 100 Jy. The black curve shows the cumulated fraction of all pixels visited by ARCHEOPS.

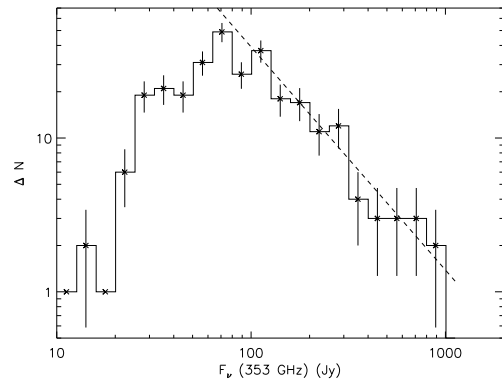


**Fig. 9.** Un-normalized number counts of the 353 GHz ARCHEOPS sources. Error bars in each histogram bin are assumed to follow a Poisson law. A best-fit power law with an exponent of  $-1.5 \pm 0.2$  is traced as the dashed line. Incompleteness starts below 100 Jy flux.

Fig. 11, where the  $1-\sigma$  confidence level contour is plotted for each source. We have to assess whether the observed  $\beta-T$  trend can be completely due to the natural correlation of errors. For this purpose, we parametrize the trend with a simple power-law:

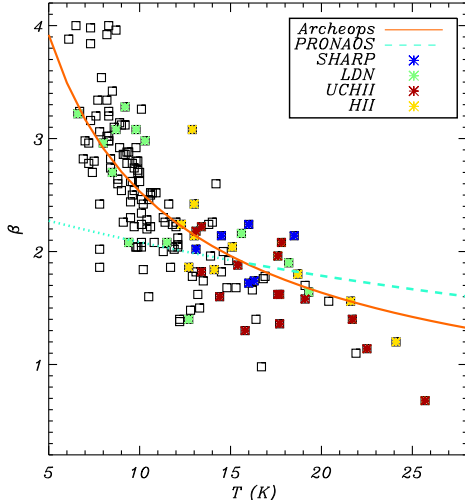
$$\beta = AT^{-\gamma}. \quad (4)$$

Fig. 12 represents the  $1, 2, 3 \sigma$  confidence level marginalized over  $T$  for the likelihood in the  $A-\gamma$  plane. A constant  $\beta$  value ( $\gamma = 0$ ) is clearly excluded at better than 99.9 % C.L.

The best fit is given by the empirical law:

$$\beta = (11.5 \pm 3.8) \times T^{-0.66 \pm 0.054}, \quad (5)$$

with error bars, after marginalization, at the 0.997 C.L. The standard  $\beta = 2$  is obtained for  $T = 14.1$  K. This law is overplotted (solid line) in Fig. 10. This inverse  $\beta-T$  relationship could also be biased by the selection of the IRAS counterparts to the ARCHEOPS sources. To prove that this is not



**Fig. 10.** Dust emissivity exponent  $\beta$  vs. temperature  $T$  for the ARCHEOPS sources (black squares). With red, green and blue stars we represent those ARCHEOPS sources identified as UCHII (ultra-compact HII), SHARP (Sharpless HII) and LDN (Lynds Dark Nebulae) sources respectively. With the orange solid line and light blue dashed line we overplot the ARCHEOPS and PRONAOS  $\beta$ - $T$  relationships as discussed in the text.

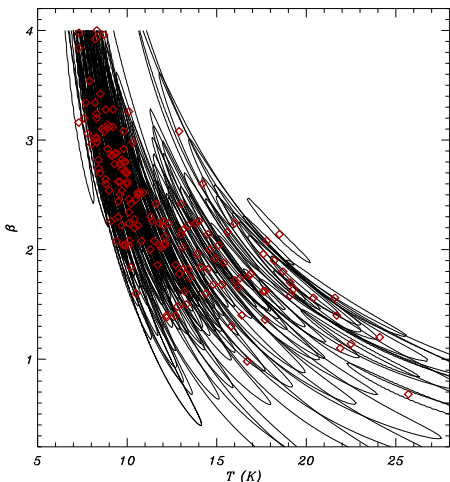


**Fig. 11.** Likelihood contour plot in a  $\beta$ - $T$  plot. Around each point source, a contour gives an uncertainty equivalent to a  $2\sigma$  level. Note that the correlation between the 2 parameter uncertainties makes it difficult to ascertain the true correlation between the parameters.

the case, we have obtained the IRAS fluxes at the position of the Archeops sources by applying the ARCHEOPS map-based source extraction algorithm (see Sect. 2.5) to the IRIS maps (Miville-Deschénes & Lagache, 2005). These fluxes were then used to repeat the fit to the spectrum of each of the ARCHEOPS sources as above. The new fit leads to the same conclusions. Dupac et al. (2003) have also claimed an anticorrelation between  $\beta$  and  $T$  for dust sources with temperatures in the range 12–20 K, as measured with the PRONAOS balloon experiment. For comparison we trace (with a dashed line, and a dotted line

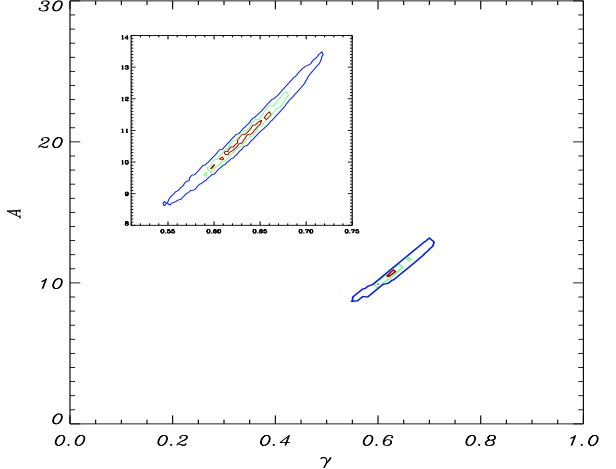


**Fig. 12.** Likelihood diagram in the  $A$ - $\gamma$  parameter plane (see Eq. 4) marginalized over  $T$ . Contours correspond to the 0.68, 0.95, 0.9999 C.L.  $\gamma = 0$  is excluded by the data at more than 0.9999 C.L. indicating a real dependence between  $T$  and  $\beta$ . Embedded plot is an expanded version of the diagram centered on the maximum of the likelihood.

for the extrapolation to lower temperatures) in Fig. 10 the  $\beta$ - $T$  relationship they obtained. ARCHEOPS and PRONAOS data show a similar behavior, even though the amplitude of the variations is larger for ARCHEOPS. The inverse  $\beta$ - $T$  relationship is not explained by standard interstellar dust models and would require us to invoke specific modifications of the optical properties of the dust, such as the ones produced in amorphous disordered material, as described by Mény et al. (2007). According to such models,  $\beta$  varies not only with temperature but also with wavelength. Therefore, the slight differences observed between the  $\beta$ - $T$  relationship by the two experiments could be due to ARCHEOPS observing at longer wavelengths ( $500\mu\text{m}$ – $2\text{ mm}$ ) than PRONAOS ( $200$ – $500\mu\text{m}$ ). Note that laboratory measurements of dust analogs exist that have revealed an increase of  $\beta$  with wavelength (see Boudet et al. 2005), in qualitative agreement with the observations. The observed effect is in the opposite direction to the diffuse interstellar medium colour trend, where  $\beta$  is measured to be low at low temperatures (Lagache et al. (1998)). To measure the absolute value of the emissivity law (which is beyond the scope of this paper) and scale it to near infrared and visible values, would require an exhaustive coherent analysis combining the submillimetre and far-infrared emission properties with the near infrared extinction properties of these clouds.

#### 4.2. Submillimetre spectrum compared to far infrared IRAS colours

We check whether these very cold clumps present special features in their far-infrared IRAS colours that would make them easy to identify at high frequency. The left plot of Fig. 13 shows that the IRAS far-infrared colours of these clumps broadly lie in two regions. For large infrared fluxes, the clumps have relatively warm colours. These sources likely contain HII regions, as exemplified by the association catalog (Table 4). On the other hand, the majority of ARCHEOPS sources have far-infrared colours similar to the general galactic point-source value ( $\sim 0.2$ ). More quantitatively, in the right plot of Fig. 13, we show the normalized his-

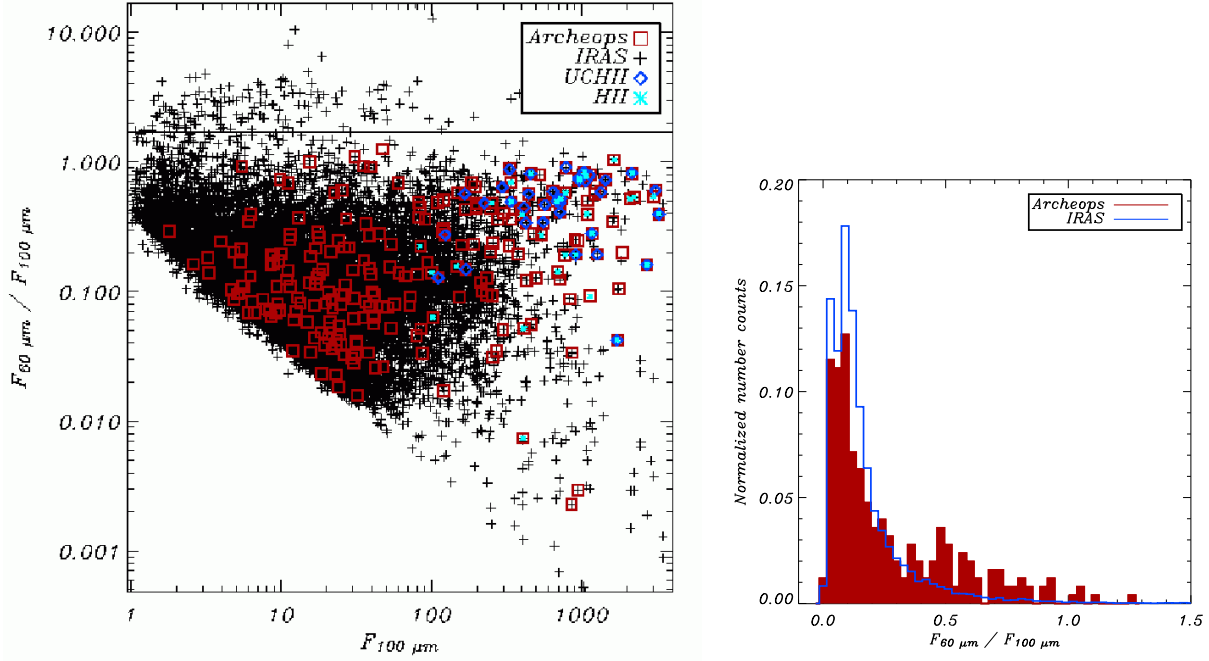


**Fig. 13.** Left plot: Far infrared IRAS colour of point sources as a function of 100 μm IRAS flux. The pluses correspond to the whole IRAS point-source catalog at low galactic latitudes ( $|b| < 10$  deg.) with detections at both 60 and 100 μm. The red squares are the IRAS colours of ARCHEOPS point-sources (when detected in IRAS). HII regions are concentrated on high fluxes and warm colours. Right plot: Histogram of the far infrared IRAS colour for the whole IRAS catalogue (blue) of point sources at low galactic latitudes ( $|b| < 10$  deg.) with detections at both 60 and 100 μm and for the subsample of ARCHEOPS point-sources (red-filled). The warm colour excess in the ARCHEOPS distribution is due to HII regions.

togram of the far infrared IRAS colours for the  $|b| \leq 10$  deg IRAS point-sources catalogue (light blue) with respect to the histogram of ARCHEOPS sources (red-filled). We observe that the distribution of the ARCHEOPS point-sources is similar to that of the Galactic IRAS point-sources with an excess of ARCHEOPS sources on the warm IRAS side.

We trace in the upper plot of Fig. 14, the far infrared IRAS colours for the Archeops sources as a function of temperature  $T$ . The far infrared IRAS colours of the ARCHEOPS sources seem to be uncorrelated with the submillimetre temperature. For most of the sources, one dust component cannot simultaneously explain the submillimetre and far-infrared colours. On the contrary, in the lower plot of Fig. 14, a single dust component is able to explain the submillimetre colours, albeit with a surprisingly large emissivity index. Therefore the far-infrared 60 to 100 μm ratio is not representative of the submillimetre dust temperature. Several dust components are needed for most sources to explain the infrared and submillimetre spectra together.

From this analysis, we find that the ARCHEOPS sources show no distinct features in their far infrared IRAS colours, except for the UCHII subpopulation. This indicates that we cannot easily predict the fluxes at submillimeter frequencies of known IRAS point-sources. Only  $\sim 1.3\%$  of the IRAS sources at low galactic latitudes ( $|b| \leq 10^\circ$ ) are detected by ARCHEOPS with a flux  $F_\nu(353 \text{ GHz}) \geq 50 \text{ Jy}$ .

Furthermore, a significant fraction ( $\sim 10\%$ ) of ARCHEOPS point-sources are not associated with any IRAS point-source making it even more difficult to estimate the point-source properties in future submillimeter surveys like PLANCK HFI.

#### 4.3. Ultra compact HII regions.

Forty ARCHEOPS sources are associated with ultra compact HII regions (UCHII, see Sect. 3.1). These regions are of particular physical interest as they are formed by young stars in the first steps of their evolution.

In Fig. 10 we show as red stars the best-fit temperature  $T$  and dust spectral index  $\beta$  for the ARCHEOPS sources associated with compact or ultra compact HII regions. We consider only those sources for which the  $T$ - $\beta$  fit satisfies the  $\chi^2$  goodness-of-fit criteria at 95% C.L.: 23 out of 66. Across the whole temperature range, we observe that these sources follow the general  $\beta$ - $T$  relationship described in Sect. 3.3:  $\beta$  increases for decreasing  $T$ . However, these sources seem to be always hotter than 13 K, likely an effect of the far-infrared selection. Note that the free-free emission does not seem to perturb the low-frequency part of the spectrum in these sources.

We also paid attention to other types of sources like dark Lynds Nebulas (LDN) and Sharpless HII regions. The best-fit temperature  $T$  and dust spectral index  $\beta$  for the ARCHEOPS sources associated with them are also represented in Fig. 10 as green and blue stars for the LDN and the Sharpless HII regions respectively. The ARCHEOPS point-sources associated with Sharpless HII regions tend to be hotter than 13 K, similarly to UCHII regions. The clouds associated with LDNs seem to be preferentially at low temperatures ( $T < 15$  K) but they follow the general  $T$ - $\beta$  relationship.

The fact that the submillimeter properties of the HII-associated clumps are not changed (except that they are hotter) may be interpreted in the following way: the submillimetre clumps could be thought of as some precursor stage of the

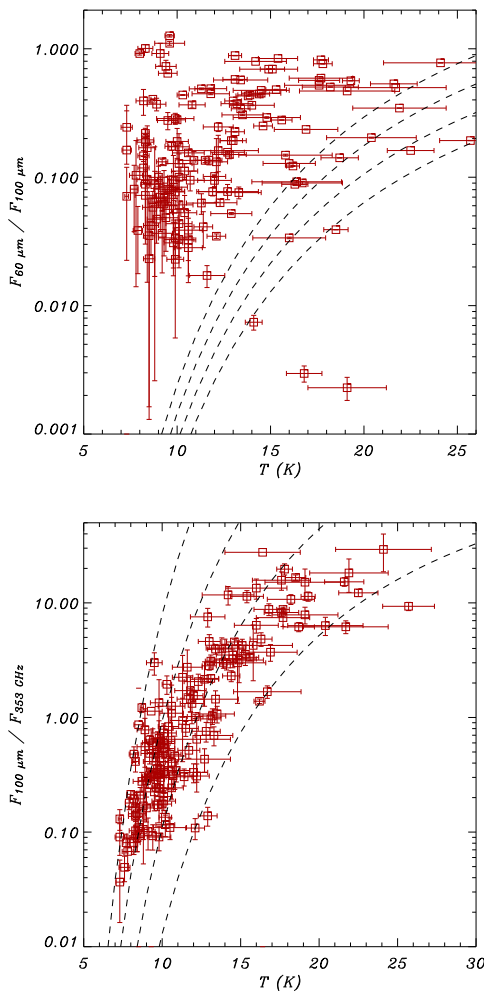


**Fig. 14.** Upper plot: Far infrared IRAS colour as a function of  $T$  for the ARCHEOPS point sources detected at  $60$  and  $100\,\mu\text{m}$ . Dashed lines in the two plots correspond to single temperature component models with an emissivity index of  $1, 2, 3, 4$ , from bottom to top. The two points at the lower right of the lines are due to an incorrect association with a  $60\,\mu\text{m}$  source. Lower plot: Submillimetre colour ( $100\,\mu\text{m}$  to  $353\,\text{GHz}$  flux ratio) of ARCHEOPS point sources with a detection at  $100\,\mu\text{m}$ , as a function of  $T$  for an acceptable fit of the spectral energy distribution.

site for massive star production. Some of those clumps have already started producing massive stars but those massive stars have not modified the global properties of the clump enough (except through radiative heating), perhaps because they have escaped from the cloud, or because the cloud is much more massive than the stellar cores themselves and hence, the cloud has not been disturbed yet.

#### 4.4. Number counts

In Sect. 3.4, we have seen that a power law exponent of  $1.5 \pm 0.2$  gives a fair representation of the integral number counts. The integrated flux of these clumps (see Eq. 3) is thus dominated by the faint sources. Because the submillimetre emission is opti-

cally thin, we can directly transform the submillimeter flux  $F_\nu$  into a total clump gas mass using the following formula:

$$M_{\text{gas}} = \frac{F_\nu D^2}{\kappa_\nu B_\nu(T)} = 1.4 \times 10^3 M_\odot \left( \frac{F_\nu(353\,\text{GHz})}{100\,\text{Jy}} \right) \left( \frac{D}{1\,\text{kpc}} \right)^2, \quad (6)$$

where  $B_\nu(T)$  is the Planck function and  $D$  is the distance to the source. The last equality is obtained with the dust absorption coefficient  $\kappa_\nu$  taken as  $0.0012\,\text{m}^2\cdot\text{kg}^{-1}$  (Preibisch et al., 1993) at  $353\,\text{GHz}$  and an assumed average dust temperature  $T$  of  $14\,\text{K}$ .

Hence, for a distance range of  $200\,\text{pc}$  to  $2\,\text{kpc}$  the detected clumps have a mass range from  $40$  to  $40,000\,M_\odot$ , intermediate between cores and giant molecular clouds. The ARCHEOPS beam encompasses  $3.5\,\text{pc}$  at a distance of  $1\,\text{kpc}$ , a "typical" intermediate size too. The likely dispersion in the distance of the different clumps prevents an interpretation of the flux number counts in terms of mass distribution and favors approaching an Euclidian count with an exponent of  $1.5$ . For example, clumps close to Cygnus are likely at a distance of  $1.7\,\text{kpc}$  (Schneider et al., 2006). Other clumps close to Taurus and Perseus associations are typically at a distance of about  $200 \pm 60\,\text{pc}$  (Dame et al. (2001)). Optical depth effects are not likely to play a major role in the fitting of Eq. 1 because a typical mass of  $1,000\,M_\odot$  extending over  $1\,\text{pc}$  has an opacity of  $0.01$  only at  $545\,\text{GHz}$  (using  $\tau = 4\kappa_\nu M_{\text{gas}} / (\pi D^2)$ ).

The satellite PLANCK (The Planck collaboration, 2005) with a thousand-fold increase in sensitivity should supersede the present results. In the mean time, the number counts allow us to firmly establish that there will be enough bright point-sources to reconstruct and monitor the PLANCK HFI (Lamarre, et al. 2003) focal plane geometry. Indeed, each detector has an instantaneous sensitivity between  $1$  and  $2\,\text{Jy}$  per acquired sample (about  $5\,\text{milliseconds}$  of integration). The sources above  $100\,\text{Jy}$  will thus be detected with an excellent signal to noise ratio at each crossing. As the scans will drift by typically one degree per day, hundreds of sources will be available for accurate astrometry of the HFI detectors during the course of the PLANCK survey, roughly one every day, and probably more when crossing the inner Galaxy.

Moreover, a deep unbiased all-sky survey of submillimetre clumps will be available at the end of the PLANCK survey. With a final HFI sensitivity of about  $10\text{--}50\,\text{mJy}$  ( $1\sigma$ ), by extrapolating ARCHEOPS number counts to the whole galaxy and to fainter fluxes, one can expect PLANCK to detect tens of thousands of submillimetre sources, actually down to the confusion limit, in the Galactic Plane.

## 5. Conclusions

This is a systematic extraction of the point sources from the ARCHEOPS last flight data. These point sources are valuable for the number counts of galactic sources in the (sub)millimetre domain and the study of the early star formation processes. The mean integration time per source is only of few tenths of seconds. Nevertheless, this shallow but wide survey has uncovered many new members of the family of very cold galactic clumps.

In general the ARCHEOPS point-sources can be associated with sources in the IRAS point-source catalogue or the IRAS small extended source catalogue. Only 30 ARCHEOPS point-sources out of a total of 304 remain unidentified.

The spectral energy distribution of the ARCHEOPS point-sources is compatible with a modified black body having as parameters the temperature  $T$  and dust spectral index  $\beta$ . By fitting the spectrum of the ARCHEOPS sources to such a model we find

that most ARCHEOPS point-sources are cold clumps with temperatures in the range of 7 to 27 K. We also prove that there exists an inverse relationship between  $T$  and  $\beta$ :  $\beta$  increases significantly with decreasing  $T$ .

We have found that most of the 302 ARCHEOPS point-sources have standard galactic IRAS far infrared colours, except for 40 identified as ultra compact HII regions, and 26 identified with other HII regions. Most of the clumps do not seem to be disturbed yet by internal sources. The far infrared colours are uncorrelated with the temperature deduced from the submillimetre fit. Only  $\sim 1.3\%$  of the IRAS sources at low galactic latitudes ( $|b| \leq 10^\circ$ ) have a bright submillimetre counterpart ( $F_\nu(353\text{ GHz}) \geq 50\text{ Jy}$ ). This means that it is difficult to predict which IRAS source will be detected in submillimetre surveys, for example, in PLANCK simulation of foreground to the CMB anisotropies.

*Acknowledgements.* The HEALPix package has been used throughout the data analysis (Gorski et al. (2005)). This research has made use of the VizieR catalogue access tool, CDS, Strasbourg, France. We thank the ARCHEOPS collaboration for their efforts throughout the long campaigns. This work has been done with the PLANCK HFI data processing facility. We thank Bruno Bezard and Raphaël Moreno for very fruitful discussions about planets.

## References

- Baars J. W. M. et al. , 1977, A&A, 61, 99  
 Beichman, C. A., Neugebauer, G., Habing, H. J., Clegg, P. E., & Chester, T. J.. 1988, Infrared astronomical satellite (IRAS) catalogs and atlases. Vol. 1: Explanatory supplement  
 Benoît, A. et al. 2002, Astropart. Phys., 17, 101  
 Benoît A. et al. 2003a, A&A, 399, No. 3, L19  
 Benoît A. et al. 2003b, A&A, 399, No. 3, L25  
 Benoît, A., et al. 2004, A&A, 424, 571  
 Bernard, J. P., 2004, 35th COSPAR Scientific Assembly, 4558  
 Boudet N., Mutschke H., Nayral C., Jäger C., Bernard J.-Ph., Henning T., Meny C., 2005, ApJ, 633, 272  
 Chini, R., Kreysa, E., Mezger, P. G., & Gemünd, H.-P., 1984, A&A, 135, L14  
 Chini, R., Kreysa, E., Mezger, P. G., & Gemünd, H.-P., 1986, A&A, 154, L8  
 Chini, R., Kreysa, E., Mezger, P. G., & Gemünd, H.-P., 1986, A&A, 157, L1  
 Dame, T. M., Hartmann, D., & Thaddeus, P., 2001, ApJ, 547, 792  
 Dunne, L., Eales, S., Ivison, R., Morgan, H., & Edmunds, M., 2003, Nature, 424, 285  
 Dupac, X. et al. , 2003, A&A, 404, L11-L15  
 Dwek, E., 2004, ApJ, 607, 848  
 Finkbeiner, D. P., Davis, M., Schlegel, D. J., 1999, ApJ, 524, 867  
 Goldin, A. B. et al. , 1997, ApJ, 488, L161  
 Gomez, H. L., Dunne, L.; Eales, S. A., Gomez, E. L., & Edmunds, M. G. 2005, MNRAS, 361, 1012  
 Gorski, K. M., Hivon, E., Banday, A. J., et al. , 2005, ApJ, 622, 759 (<http://healpix.jpl.nasa.gov>)  
 Green, D. A., 2004, Bull. Astr. Soc. India, 2004, 32, 335, updates at (<http://www.mrao.cam.ac.uk/surveys/snrs>)  
 Hernández-Monteagudo, C., Macías-Pérez, J.F., Tristram, M. & Désert, F.-X., 2006, A&A, 449, 41–48  
 Hinshaw, G., Nolta, M. R., Bennett, C. L., et al. 2007, ApJS, 170, 288  
 Kurtz, Churchwell & Wood, 1994, ApJ, 91, 659  
 Lagache, G., Abergel, A., Boulanger, F., & Puget, J.-L., 1998, A&A, 333, 709L  
 Lamarre, J.-M., Puget, J.-L., Piat, M., et al. , 2003, in Proceedings of the SPIE, IR Space Telescopes and Instruments, J. C. Mather (Ed.), 4850, 730  
 Macías-Pérez, J., Lagache, G., Maffei, B., et al. 2007, A&A, 467, 1313  
 Macías-Pérez, J.F., Mayet, F., Désert, F.-X. & Aumont, J., 2008a, A&A, companion paper, submitted  
 Macias-Perez, J.F., Mayet, F., Désert, F.-X., 2008b, in preparation  
 Miville-Dechênes, M.-A. & Lagache, G., 2005, ApJS, 157, 302-323  
 Meny, C., Gromov, V., Boudet, N., et al. , 2007, A&A, 468, 171  
 Moreno, R., 1998, PhD Thesis, Université Paris VI  
 Pajot, F., Stepnik, B., Lamarre, J.-M., et al. , 2006, A&A, 447, 769  
 Page, L., Barnes, C., Hinshaw, G., Spergel, D. N., Weiland, J. L., et al., 2003, ApJS, 148, 39  
 Paladini, R., Burigana, C., Davies, R. D., Maino, D., Bersanelli, M. et al. , 2003, A&A, 397, 213  
 The Planck collaboration. 2005,  
 Available at:  
[http://www.rssd.esa.int/SA/PLANCK/docs/Bluebook-ESA-SCI\(2005\)1\\_V2.pdf](http://www.rssd.esa.int/SA/PLANCK/docs/Bluebook-ESA-SCI(2005)1_V2.pdf)  
 Ponthieu, N., Macías-Pérez, J. M., Tristram, M., et al. 2005, A&A, 444, 327  
 Preibisch, Th., Ossenkopf, V., Yorke, H. W., & Henning, Th., 1993, A&A, 279, 577  
 Schneider, N., Bontemps, S., Simon, R., et al. , 2006, A&A, 458, 855  
 Tristram, M., Patanchon, G., Macías-Pérez, J.F. et al. 2005, A&A, 436, 785

**Table 3.** Archeops point-source catalog. The name of the source gives the galactic coordinates in degrees. Fluxes and  $1-\sigma$  errors are in Jy, assuming a Rayleigh-Jeans color and for the 4 frequencies of 143, 217, 353 and 545 GHz. No available measurements are quoted as  $\sigma = -1$ . Upper limits are quoted at the  $2-\sigma$  level. The bright sources with an asterisk have positional uncertainties larger than the nominal 4 arcmin. ( $1-\sigma$ , see Sect. 2.5).

N	Name	RA (2000)	Dec (2000)	$F_{143}$	$\sigma_{143}$	S/N	$F_{217}$	$\sigma_{217}$	S/N	$F_{353}$	$\sigma_{353}$	S/N	$F_{545}$	$\sigma_{545}$	S/N
1	ArchG063.36+11.11	19 06 19.8	+32 01 15	< 6.7	3.3	< 2	22.7	4.4	5	66	11	6	201	95	2
2	ArchG073.55+02.63	20 05 59.7	+36 51 01	< 6.4	3.2	< 2	24.0	4.0	6	116	23	5	0	-1	0
3	ArchG075.75+00.33	20 21 40.8	+37 24 44	50.4	7.8	6	150.4	11.9	13	0	-1	0	0	-1	0
4	ArchG075.97+00.69	20 20 49.6	+37 47 51	18.7	3.7	5	23.0	9.2	2	0	-1	0	1940	67	29
5	ArchG076.81+02.14	20 17 08.4	+39 18 22	11.4	3.2	4	52.5	6.5	8	88	28	3	584	78	7
6	ArchG077.35+01.83	20 20 00.2	+39 34 36	13.9	2.0	7	76.0	8.3	9	266	21	13	1578	46	34
7	ArchG077.59+00.62	20 25 51.0	+39 05 09	< 7.0	3.5	< 2	41.5	5.7	7	0	-1	0	554	95	6
8	ArchG077.88+01.78*	20 21 47.5	+39 59 04	14.9	2.7	6	58.6	8.2	7	319	25	12	1883	75	25
9	ArchG077.95-00.14	20 30 06.7	+38 55 52	< 8.4	4.2	< 2	39.0	6.5	6	0	-1	0	1695	135	13
10	ArchG078.11-00.50	20 32 07.6	+38 51 01	40.3	7.8	5	75.9	10.3	7	0	-1	0	0	-1	0
11	ArchG078.17+03.95	20 13 10.2	+41 26 16	13.4	3.3	4	27.7	4.5	6	91	11	8	451	95	5
12	ArchG078.50+01.05	20 26 47.4	+40 04 02	29.5	2.6	12	109.3	3.6	31	0	-1	0	1531	92	17
13	ArchG079.15+02.22	20 23 44.5	+41 16 56	13.2	3.1	4	74.5	8.6	9	205	15	13	1350	92	15
14	ArchG079.22+00.28	20 32 15.3	+40 12 02	18.7	2.9	6	76.4	3.0	25	512	57	9	1819	92	20
15	ArchG079.37+00.94	20 29 56.0	+40 42 47	< 5.4	2.7	< 2	20.5	6.2	3	249	22	11	1372	78	18
16	ArchG079.37+01.20*	20 28 48.1	+40 52 20	9.8	2.0	5	74.5	4.6	16	178	14	13	1838	53	34
17	ArchG079.43+03.37	20 19 31.3	+42 09 45	< 7.9	4.0	< 2	58.2	6.3	9	267	10	26	954	130	7
18	ArchG079.57+03.57	20 19 00.4	+42 23 34	3.9	1.8	2	24.3	3.2	8	0	-1	0	334	55	6
19	ArchG079.69+01.12*	20 30 07.8	+41 04 48	10.3	2.2	5	59.2	4.5	13	132	14	9	1812	58	31
20	ArchG079.90+02.54	20 24 37.1	+42 04 20	7.3	2.6	3	52.9	3.7	14	257	22	11	0	-1	0
21	ArchG080.51+03.32	20 23 01.9	+43 01 15	4.9	2.4	2	21.3	4.0	5	< 62	31	< 2	268	51	5
22	ArchG080.89+00.30*	20 37 28.4	+41 33 28	15.1	2.4	6	73.6	5.6	13	295	14	20	1663	92	18
23	ArchG080.91-00.14	20 39 22.4	+41 18 11	28.3	2.8	10	89.5	3.0	30	0	-1	0	2293	92	25
24	ArchG081.24+00.57*	20 37 27.4	+41 59 50	< 5.6	2.8	< 2	52.9	5.2	10	167	14	12	2208	75	29
25	ArchG081.26+01.12*	20 35 07.7	+42 20 28	29.6	2.4	12	80.4	3.1	26	353	25	14	1216	92	13
26	ArchG081.59+03.03	20 27 48.0	+43 44 20	9.1	1.7	5	12.9	2.9	4	0	-1	0	390	55	7
27	ArchG081.67+00.53	20 39 02.9	+42 18 55	41.3	2.7	15	159.2	5.9	27	727	14	49	4587	65	70
28	ArchG081.68+02.76*	20 29 17.2	+43 39 04	10.0	1.4	7	61.7	4.1	15	207	25	8	1071	39	27
29	ArchG081.94+02.31	20 32 07.5	+43 36 04	11.2	2.0	6	56.6	3.8	15	215	28	8	1120	40	27
30	ArchG082.48+00.16	20 43 17.4	+42 43 47	< 5.2	2.6	< 2	31.0	5.7	5	69	19	4	417	78	5
31	ArchG082.93+03.38	20 30 32.6	+45 01 33	6.5	1.9	3	23.0	4.0	6	< 57	28	< 2	256	45	6
32	ArchG083.04+01.93	20 37 29.8	+44 15 13	< 3.4	1.7	< 2	22.4	2.7	8	108	21	5	631	55	11
33	ArchG083.61-02.12	20 56 44.5	+42 09 08	< 4.8	2.4	< 2	31.1	4.9	6	0	-1	0	855	51	17
34	ArchG083.75+03.31	20 33 37.9	+45 38 59	14.1	1.6	9	37.0	2.7	14	217	14	15	607	53	11
35	ArchG084.64+00.18	20 50 42.0	+44 25 37	17.9	1.4	13	61.1	2.3	27	308	14	22	972	49	20
36	ArchG084.79-01.15	20 56 54.6	+43 40 48	24.5	1.3	18	113.0	2.4	47	604	16	38	2543	37	67
37	ArchG084.82+01.59	20 45 08.1	+45 27 09	4.9	2.1	2	22.5	3.6	6	76	17	4	393	55	7
38	ArchG084.84+03.86	20 34 49.5	+46 50 58	10.5	1.3	8	27.8	3.3	8	139	15	9	564	36	16
39	ArchG084.96-00.39	20 54 18.9	+44 18 12	< 3.3	1.7	< 2	41.7	3.2	13	146	12	12	828	49	17
40	ArchG085.14+03.94	20 35 29.5	+47 07 56	11.5	1.5	8	33.6	2.4	14	90	11	8	563	49	11
41	ArchG085.45+02.73	20 42 13.8	+46 38 37	< 3.0	1.5	< 2	12.8	2.6	5	79	11	7	413	37	11
42	ArchG086.41+00.44	20 56 00.5	+45 57 10	< 2.9	1.4	< 2	18.2	2.8	6	80	18	4	186	31	6
43	ArchG086.65+00.38	20 57 11.7	+46 05 35	5.2	1.4	4	16.6	2.8	6	68	10	6	139	33	4
44	ArchG086.72+05.30	20 34 35.3	+49 12 38	< 3.2	1.6	< 2	9.7	3.1	3	78	14	5	361	47	8
45	ArchG087.30+04.05	20 42 46.1	+48 55 09	< 3.7	1.8	< 2	9.4	2.9	3	61	11	6	265	51	5
46	ArchG089.30-00.04	21 09 20.5	+47 47 24	< 3.3	1.7	< 2	21.4	2.7	8	124	18	7	< 156	78	< 2
47	ArchG089.57+02.09	21 00 48.6	+49 24 58	9.0	1.8	5	21.0	3.0	7	89	20	4	336	95	4
48	ArchG089.93-01.97	21 20 06.7	+46 54 40	3.8	1.8	2	18.9	3.1	6	108	12	9	627	51	12
49	ArchG090.39+02.32	21 03 08.2	+50 11 01	4.7	1.5	3	21.7	2.5	9	102	18	5	708	40	17
50	ArchG090.97+01.49	21 09 24.5	+50 03 15	7.1	1.9	4	28.0	2.8	10	84	11	8	507	60	8
51	ArchG091.10+01.77	21 08 40.1	+50 20 15	< 3.3	1.6	< 2	15.4	2.7	6	< 44	22	< 2	312	55	6
52	ArchG091.32-00.30	21 18 52.6	+49 04 08	< 3.6	1.8	< 2	17.8	3.1	6	98	17	6	408	78	5
53	ArchG092.03+03.93	21 02 19.8	+52 28 39	10.3	1.1	9	37.6	1.8	21	178	15	11	1031	39	26
54	ArchG092.22+02.85	21 08 24.3	+51 53 36	< 3.3	1.6	< 2	18.1	2.5	7	79	13	6	405	51	8
55	ArchG092.57+04.61	21 01 20.0	+53 19 44	< 3.2	1.6	< 2	6.6	3.1	2	64	10	6	394	40	10
56	ArchG092.90+04.05	21 05 36.1	+53 12 15	4.2	1.7	2	15.2	2.6	6	36	14	3	397	60	7
57	ArchG093.10+02.79*	21 12 37.4	+52 29 53	12.5	1.0	12	32.1	2.8	11	97	8	12	319	31	10
58	ArchG093.40-00.15	21 27 26.5	+50 38 15	< 3.5	1.8	< 2	21.1	4.0	5	53	18	3	298	32	9
59	ArchG093.78+01.91	21 19 53.9	+52 22 21	5.4	1.6	3	20.4	3.4	6	79	12	6	273	37	7
60	ArchG094.01+09.86	20 38 40.8	+57 43 45	< 3.0	1.5	< 2	6.2	2.5	2	51	9	5	226	36	6
61	ArchG094.38-05.46	21 53 15.4	+47 17 35	< 4.5	2.3	< 2	32.0	3.3	10	168	24	7	759	95	8
62	ArchG094.56-00.06	21 32 24.1	+51 30 18	< 3.6	1.8	< 2	16.4	2.7	6	43	18	2	357	55	6
63	ArchG095.62-00.76	21 40 29.9	+51 41 38	< 3.8	1.9	< 2	< 7.2	3.6	< 2	67	12	5	470	55	9
64	ArchG096.05+08.02	20 59 00.3	+58 10 23	< 2.6	1.3	< 2	10.3	2.0	5	59	9	6	232	37	6
65	ArchG096.26-00.14	21 40 58.1	+52 34 32	5.9	1.4	4	18.4	2.5	7	50	9	5	255	34	7
66	ArchG097.32+09.90	20 53 55.2	+60 20 36	3.8	1.2	3	8.2	2.1	4	77	10	7	251	40	6
67	ArchG097.44+03.25	21 31 23.1	+55 53 11	7.9	1.5	5	21.7	2.5	9	75	13	5	609	36	17
68	ArchG097.68+03.18*	21 33 02.2	+55 59 50	5.6	1.4	4	18.4	1.8	10	673	9	74	311	53	6
69	ArchG097.82+08.67	21 04 02.7	+59 55 30	< 2.8	1.4	< 2	13.5	2.6	5	51	15	3	222	36	6

**Table 3.** continued.

N	Name	RA (2000)	Dec (2000)	$F_{143}$	$\sigma_{143}$	S/N	$F_{217}$	$\sigma_{217}$	S/N	$F_{353}$	$\sigma_{353}$	S/N	$F_{545}$	$\sigma_{545}$	S/N
70	ArchG098.00+01.55	21 42 22.7	+54 59 52	11.3	1.2	10	36.7	2.1	17	111	16	7	706	36	19
71	ArchG098.35+06.11	21 21 30.2	+58 33 58	< 3.0	1.5	< 2	11.8	2.2	5	52	9	6	152	51	3
72	ArchG098.43+13.79	20 32 52.4	+63 31 52	< 2.5	1.2	< 2	10.5	1.9	5	42	7	5	180	29	6
73	ArchG099.11+00.69	21 52 09.2	+55 02 20	< 2.8	1.4	< 2	14.1	2.8	5	< 32	16	< 2	349	40	9
74	ArchG099.13+01.00	21 50 54.1	+55 17 33	< 3.2	1.6	< 2	14.7	2.7	5	29	9	3	343	47	7
75	ArchG099.37+01.27	21 51 02.4	+55 39 37	< 2.7	1.4	< 2	14.4	2.7	5	56	18	3	165	32	5
76	ArchG100.01+04.26	21 40 26.4	+58 21 15	4.3	1.4	3	21.3	2.0	11	107	10	10	464	36	13
77	ArchG100.16+03.02	21 47 18.9	+57 30 48	< 3.1	1.6	< 2	12.6	2.2	6	54	10	5	141	45	3
78	ArchG100.22+02.06	21 52 10.8	+56 48 45	< 2.6	1.3	< 2	11.8	2.3	5	37	11	3	159	26	6
79	ArchG100.35+03.35	21 46 51.8	+57 53 29	< 2.9	1.5	< 2	13.1	2.2	6	105	9	11	469	34	13
80	ArchG100.44+08.84	21 17 20.3	+61 57 18	< 2.3	1.1	< 2	10.7	1.9	6	59	10	6	213	34	6
81	ArchG100.57+16.40	20 22 29.9	+66 40 55	< 1.6	0.8	< 2	6.0	1.2	5	31	6	5	0	-1	0
82	ArchG101.41+02.59	21 56 40.7	+57 57 49	< 4.0	2.0	< 2	13.9	2.7	5	74	9	8	169	55	3
83	ArchG101.63+11.17	21 09 08.3	+64 23 50	< 2.4	1.2	< 2	11.1	1.7	7	33	7	4	179	31	6
84	ArchG101.96-00.21	22 12 05.0	+56 01 47	< 3.2	1.6	< 2	17.6	2.8	6	< 42	21	< 2	253	42	6
85	ArchG102.08+11.11	21 12 20.8	+64 41 08	< 1.8	0.9	< 2	< 3.1	1.6	< 2	38	7	5	167	24	7
86	ArchG102.16+15.35	20 40 06.9	+67 23 47	< 3.3	1.7	< 2	28.1	3.8	7	65	11	6	0	-1	0
87	ArchG102.35+08.32	21 32 05.8	+62 55 31	< 2.2	1.1	< 2	9.9	1.9	5	< 28	14	< 2	184	29	6
88	ArchG102.69+08.43	21 33 35.5	+63 13 52	2.8	1.0	3	11.8	1.7	7	57	10	5	204	28	7
89	ArchG102.71-00.78*	22 18 50.2	+55 59 09	9.2	1.6	6	26.3	3.2	8	149	11	13	554	43	13
90	ArchG102.80+02.13	22 07 10.6	+58 25 33	< 2.5	1.3	< 2	13.2	2.3	6	44	18	2	383	37	10
91	ArchG103.43+13.69	21 01 34.2	+67 22 22	3.7	1.6	2	13.0	1.9	7	36	4	9	0	-1	0
92	ArchG103.73+02.18	22 12 47.3	+59 00 15	4.4	1.3	3	25.0	2.4	11	112	10	11	455	37	12
93	ArchG103.97+10.93	21 25 49.6	+65 54 29	3.4	0.8	4	9.6	1.2	8	57	7	8	186	22	8
94	ArchG104.10+12.23	21 17 19.2	+66 54 09	< 1.4	0.7	< 2	9.1	1.1	8	27	5	5	0	-1	0
95	ArchG104.49+01.33	22 21 20.3	+58 42 57	6.5	1.3	5	18.8	2.1	9	77	11	7	438	60	7
96	ArchG104.66+11.38	21 27 23.4	+66 42 16	2.8	0.9	3	9.9	1.3	8	43	5	8	396	34	11
97	ArchG104.69+00.30	22 26 48.8	+57 57 37	< 3.3	1.7	< 2	14.0	2.7	5	60	9	6	225	42	5
98	ArchG104.77+02.88	22 16 29.7	+60 09 54	3.0	1.3	2	12.9	2.5	5	68	13	5	315	45	7
99	ArchG104.99+07.26	21 55 55.0	+63 50 22	< 1.8	0.9	< 2	9.1	1.8	5	27	10	3	172	26	7
100	ArchG105.39+09.89	21 42 52.3	+66 06 26	7.3	0.7	11	27.9	1.2	24	107	9	11	478	17	27
101	ArchG105.55+10.45	21 40 17.7	+66 37 58	< 0.9	0.4	< 2	11.2	1.2	9	38	5	7	304	11	26
102	ArchG105.69+00.44	22 32 45.5	+58 35 22	2.9	1.4	2	15.2	2.3	7	91	11	8	253	37	7
103	ArchG105.74+01.35	22 29 31.3	+59 23 52	< 2.5	1.3	< 2	13.7	2.3	6	36	10	3	380	40	9
104	ArchG105.89+04.17	22 18 12.8	+61 51 37	5.6	1.4	4	16.6	2.2	8	64	14	4	455	40	11
105	ArchG106.52+07.09	22 08 02.0	+64 37 19	< 2.0	1.0	< 2	5.3	1.7	3	46	7	6	139	25	5
106	ArchG106.53+01.11	22 35 52.6	+59 35 24	4.6	1.5	3	22.1	2.4	9	131	14	9	615	67	9
107	ArchG106.88+05.29	22 20 02.0	+63 20 28	28.8	0.9	31	125.2	1.4	88	664	8	79	3300	37	87
108	ArchG107.17-00.91	22 47 37.0	+58 07 15	9.0	1.4	6	21.1	2.4	9	77	12	6	489	45	11
109	ArchG107.22+00.04	22 44 39.1	+58 59 09	4.4	1.4	3	15.4	2.4	6	73	13	5	164	47	3
110	ArchG107.37+07.65	22 11 27.7	+65 33 44	< 1.8	0.9	< 2	9.1	1.4	6	41	7	6	207	23	9
111	ArchG108.11+02.75	22 40 32.7	+61 47 27	5.2	1.2	4	17.8	2.1	9	83	15	5	503	34	14
112	ArchG108.15+05.52	22 28 34.8	+64 12 33	< 2.1	1.0	< 2	9.0	1.8	5	46	8	5	168	25	7
113	ArchG108.23-01.19	22 55 49.3	+58 20 22	< 2.9	1.4	< 2	8.8	2.5	3	63	12	5	227	39	6
114	ArchG108.34+00.52	22 50 44.7	+59 55 44	3.4	1.3	3	15.6	2.3	7	36	13	3	196	34	6
115	ArchG108.63+00.45*	22 53 03.8	+59 59 42	6.8	1.4	5	26.2	1.9	14	110	10	11	677	46	15
116	ArchG108.80+01.40	22 50 52.7	+60 55 08	< 2.7	1.4	< 2	18.8	2.3	8	76	11	7	209	51	4
117	ArchG108.85-01.05	22 59 36.7	+58 43 53	6.3	1.4	5	36.5	2.6	14	146	12	12	552	49	11
118	ArchG108.89+02.69	22 46 35.2	+62 06 35	2.9	1.2	2	27.8	2.0	14	142	8	16	577	37	15
119	ArchG109.01-00.36*	22 58 32.2	+59 25 41	9.2	1.1	8	34.4	2.6	13	107	10	11	549	33	16
120	ArchG109.43+06.56	22 33 51.1	+65 45 16	15.4	0.7	22	42.6	1.2	36	197	7	27	954	22	43
121	ArchG109.51+08.77	22 22 49.3	+67 41 03	< 3.4	1.7	< 2	11.1	1.8	6	30	3	9	0	-1	0
122	ArchG109.80+08.63	22 26 08.9	+67 43 05	< 3.4	1.7	< 2	11.9	1.8	7	22	3	6	0	-1	0
123	ArchG109.82+02.17*	22 55 39.8	+62 03 26	12.9	1.2	11	59.8	1.8	34	334	11	29	1723	43	40
124	ArchG109.89+05.34	22 43 22.9	+64 55 20	< 1.1	0.5	< 2	5.8	0.8	7	53	6	8	172	20	8
125	ArchG110.26+02.46	22 58 02.9	+62 30 34	9.3	1.0	9	33.8	2.0	17	140	8	17	790	36	22
126	ArchG110.50-00.42	23 09 30.6	+59 57 53	7.4	1.5	5	60.1	1.8	34	208	11	18	1045	58	18
127	ArchG110.75+05.30	22 50 50.0	+65 16 43	3.2	0.9	4	7.3	1.4	5	< 14	7	< 2	145	28	5
128	ArchG110.80+06.56	22 45 36.8	+66 25 25	< 1.4	0.7	< 2	7.8	1.1	7	25	6	4	114	22	5
129	ArchG110.87-02.84	23 19 02.5	+57 51 21	< 3.5	1.7	< 2	15.3	2.8	5	96	31	3	493	55	9
130	ArchG110.88-01.21	23 14 39.3	+59 22 48	< 4.1	2.1	< 2	18.2	2.9	6	112	18	6	206	51	4
131	ArchG110.93+03.79	22 58 29.2	+63 59 39	2.1	1.0	2	9.7	1.6	6	46	8	6	138	30	5
132	ArchG111.11-03.01	23 21 13.3	+57 46 25	< 4.0	2.0	< 2	17.4	3.6	5	110	17	6	478	60	8
133	ArchG111.29-00.68	23 16 08.9	+60 01 22	16.2	1.4	12	54.4	1.9	28	246	11	22	953	46	21
134	ArchG111.42-02.91	23 23 07.0	+57 58 19	5.5	1.2	4	32.0	3.3	10	113	18	6	672	37	18
135	ArchG111.53+00.75	23 13 45.2	+61 26 19	59.3	0.9	64	210.2	1.9	109	862	11	74	4367	27	160
136	ArchG111.70-02.13	23 23 06.4	+58 48 13	74.5	1.3	57	58.3	2.9	20	121	14	8	359	36	10
137	ArchG111.87+05.99	22 57 40.6	+66 23 21	1.9	0.7	3	5.2	1.0	5	< 20	10	< 2	151	23	7
138	ArchG112.05+01.66	23 14 59.6	+62 28 29	< 2.4	1.2	< 2	10.5	2.0	5	< 36	18	< 2	258	30	9
139	ArchG112.20+05.26	23 03 36.7	+65 51 41	2.1	1.0	2	5.4	1.5	4	44	8	5	196	28	7
140	ArchG112.43+02.84	23 14 20.1	+63 42 37	2.8	1.4	2	21.2	2.0	10	84	7	11	465	31	15
141	ArchG112.76-02.05	23 30 45.7	+59 12 59	< 2.9	1.4	< 2	14.7	2.8	5	< 44	22	< 2	256	45	6

**Table 3.** continued.

N	Name	RA (2000)	Dec (2000)	$F_{143}$	$\sigma_{143}$	S/N	$F_{217}$	$\sigma_{217}$	S/N	$F_{353}$	$\sigma_{353}$	S/N	$F_{545}$	$\sigma_{545}$	S/N
145	ArchG113.61+01.77	23 27 31.1	+63 06 32	< 2.1	1.0	< 2	6.6	2.1	3	51	10	5	150	25	6
146	ArchG114.07+02.01	23 30 47.3	+63 29 06	2.9	1.0	3	11.8	1.9	6	25	11	2	244	30	8
147	ArchG114.17+06.69	23 16 26.1	+67 55 43	< 2.9	1.5	< 2	11.8	2.0	6	33	4	7	0	-1	0
148	ArchG114.28+05.95	23 20 20.3	+67 16 31	4.6	0.8	6	14.7	1.4	10	38	7	5	0	-1	0
149	ArchG114.31+06.18	23 19 45.1	+67 30 05	2.3	0.7	3	14.5	0.7	21	38	4	8	0	-1	0
150	ArchG114.33+03.28	23 29 25.7	+64 46 16	< 2.2	1.1	< 2	5.7	1.8	3	42	8	5	210	33	6
151	ArchG114.38+01.07	23 35 51.7	+62 40 38	< 2.4	1.2	< 2	9.2	1.9	5	60	11	5	273	45	6
152	ArchG114.52-00.47	23 40 39.7	+61 14 18	5.2	1.4	4	25.0	2.4	10	106	12	9	426	42	10
153	ArchG115.15+05.30	23 30 49.5	+66 56 54	< 1.3	0.6	< 2	5.5	1.4	4	45	7	6	201	13	15
154	ArchG115.24+02.54	23 39 32.1	+64 19 43	2.7	1.1	2	11.8	1.6	7	72	7	9	428	45	10
155	ArchG115.24-01.46	23 48 27.5	+60 27 53	6.0	1.6	4	18.8	2.7	7	89	22	4	465	36	13
156	ArchG115.47+05.75	23 32 35.1	+67 28 28	< 1.3	0.7	< 2	6.1	1.0	6	35	6	5	0	-1	0
157	ArchG115.83+03.97	23 41 11.7	+65 51 48	< 1.8	0.9	< 2	16.8	1.6	11	62	9	7	196	27	7
158	ArchG115.83-03.06	23 55 52.4	+59 02 46	< 3.9	1.9	< 2	17.0	3.6	5	76	14	5	464	67	7
159	ArchG115.86+06.18	23 35 12.1	+67 59 59	7.5	1.8	4	17.4	1.8	9	70	4	17	0	-1	0
160	ArchG115.92-01.62	23 54 05.6	+60 27 56	7.8	1.6	5	31.9	2.6	12	141	11	12	725	53	14
161	ArchG117.33+03.14	23 57 11.0	+65 25 15	7.4	1.0	8	29.7	1.6	19	129	8	15	610	29	21
162	ArchG117.55+02.25	00 00 59.9	+64 35 45	3.2	1.1	3	10.1	1.7	6	49	7	6	234	31	7
163	ArchG117.75-03.52	00 11 11.0	+58 56 40	< 3.6	1.8	< 2	16.5	3.2	5	57	21	3	266	47	6
164	ArchG117.81+04.05	00 00 02.4	+66 24 24	3.8	0.6	6	17.6	1.0	17	56	11	5	268	20	13
165	ArchG118.05+04.95	00 00 34.3	+67 20 20	22.5	1.0	23	67.5	1.0	66	268	6	41	0	-1	0
166	ArchG118.81+03.06	00 11 25.8	+65 36 51	4.8	1.0	5	15.9	1.6	10	81	9	9	317	32	10
167	ArchG119.06+01.50	00 15 54.9	+64 06 15	< 2.2	1.1	< 2	9.3	1.8	5	31	9	3	183	31	6
168	ArchG119.26-01.05	00 20 28.5	+61 36 10	7.2	1.7	4	20.6	3.6	6	77	21	4	219	36	6
169	ArchG119.46-01.52	00 22 34.1	+61 09 36	< 3.3	1.7	< 2	13.0	2.6	5	98	11	9	326	42	8
170	ArchG119.61+05.25	00 16 10.4	+67 53 43	4.5	2.1	2	19.2	2.3	8	29	4	6	0	-1	0
171	ArchG119.81+03.88	00 20 03.7	+66 33 43	1.6	0.7	2	6.1	1.2	5	65	8	8	152	24	6
172	ArchG120.31+02.99	00 25 56.9	+65 43 40	3.1	0.9	3	28.6	1.5	19	117	10	12	568	27	21
173	ArchG120.40+01.99	00 27 40.4	+64 44 42	< 2.1	1.1	< 2	4.7	1.9	2	54	10	5	245	25	10
174	ArchG120.67+04.02	00 28 27.9	+66 47 31	< 1.5	0.7	< 2	11.9	1.5	8	35	8	4	208	20	10
175	ArchG120.67+01.20	00 30 49.3	+63 59 00	< 2.4	1.2	< 2	15.7	2.5	6	52	20	3	319	31	10
176	ArchG120.92+02.89	00 31 56.0	+65 41 02	< 2.1	1.1	< 2	8.5	1.7	5	30	9	3	231	33	7
177	ArchG121.07+01.16	00 34 29.0	+63 58 19	2.3	1.2	2	8.1	1.9	4	66	11	6	145	26	5
178	ArchG121.29+03.19	00 35 17.7	+66 00 37	1.8	0.8	2	6.6	1.3	5	20	8	2	254	32	8
179	ArchG121.76+03.99	00 39 32.6	+66 49 48	1.7	0.7	2	7.9	1.4	6	38	7	6	116	20	6
180	ArchG121.76+00.22	00 41 05.3	+63 04 15	< 2.7	1.3	< 2	17.4	2.6	7	58	28	2	226	45	5
181	ArchG121.91-01.45	00 42 53.7	+61 24 29	< 3.9	1.9	< 2	15.0	2.8	5	64	10	6	360	67	5
182	ArchG122.10+03.41	00 43 10.0	+66 16 18	3.4	0.8	4	8.4	1.3	6	23	7	3	229	23	10
183	ArchG123.01-00.89	00 52 05.3	+61 59 10	< 3.9	2.0	< 2	24.5	2.9	8	87	9	9	547	67	8
184	ArchG123.15-06.29	00 52 58.6	+56 34 37	10.0	2.5	4	32.6	4.5	7	146	14	10	850	67	13
185	ArchG123.31+02.97	00 55 05.1	+65 50 19	3.9	1.1	4	11.0	1.7	6	56	7	8	278	31	9
186	ArchG123.81+02.39	00 59 49.7	+65 14 41	2.7	0.9	3	13.2	1.4	10	46	7	6	244	41	6
187	ArchG124.06+03.41	01 02 36.7	+66 15 41	2.2	0.7	3	16.3	1.3	13	63	9	7	294	22	13
188	ArchG124.54+02.09	01 06 37.3	+64 54 57	4.3	1.4	3	18.0	2.5	7	117	18	6	551	42	13
189	ArchG124.61+02.37	01 07 25.2	+65 11 21	3.3	0.8	4	23.3	1.8	13	106	13	8	435	27	16
190	ArchG125.60+04.18	01 18 37.8	+66 54 26	< 1.8	0.9	< 2	8.1	1.6	5	< 14	7	< 2	147	22	6
191	ArchG125.91+03.22	01 20 36.6	+65 55 27	< 2.0	1.0	< 2	9.2	1.7	6	< 37	18	< 2	158	25	6
192	ArchG126.37-01.31	01 20 13.5	+61 21 52	4.2	1.9	2	10.7	3.0	4	74	14	5	305	60	5
193	ArchG126.40+00.33	01 22 05.4	+62 59 25	< 3.9	2.0	< 2	17.9	3.5	5	91	12	7	203	67	3
194	ArchG126.69-00.79	01 23 24.0	+61 51 06	14.9	1.8	8	60.2	3.0	20	268	18	14	1376	78	18
195	ArchG126.89-00.94*	01 24 54.3	+61 40 22	10.6	1.6	7	59.8	2.3	26	278	14	19	1299	58	22
196	ArchG127.34+03.60	01 35 03.2	+66 05 37	2.8	1.0	3	10.2	1.6	6	< 40	20	< 2	211	26	8
197	ArchG127.69+02.65	01 36 52.5	+65 05 58	< 2.9	1.5	< 2	12.9	2.4	5	70	12	5	< 95	47	< 2
198	ArchG127.74+01.19	01 34 58.1	+63 39 25	< 2.9	1.4	< 2	15.4	2.6	6	< 37	18	< 2	205	34	6
199	ArchG128.28+05.87	01 49 08.6	+68 08 21	9.2	1.6	6	< 4.3	2.1	< 2	24	4	5	0	-1	0
200	ArchG128.60+04.19	01 48 27.5	+66 26 12	< 1.7	0.9	< 2	7.2	1.4	5	< 46	23	< 2	268	23	11
201	ArchG128.93+04.35	01 52 02.0	+66 30 55	< 1.7	0.8	< 2	11.7	1.5	8	28	12	2	341	22	15
202	ArchG129.22-00.24	01 45 22.0	+61 58 32	< 3.4	1.7	< 2	18.4	3.1	6	< 62	31	< 2	370	45	8
203	ArchG130.39-00.83	01 53 51.0	+61 07 55	< 3.8	1.9	< 2	14.3	3.3	4	79	12	6	297	45	7
204	ArchG130.83-01.00	01 57 00.3	+60 51 58	< 3.2	1.6	< 2	17.8	2.7	7	51	15	3	247	47	5
205	ArchG133.07+00.74	02 19 09.4	+61 52 18	< 3.1	1.6	< 2	18.8	2.6	7	73	11	6	0	-1	0
206	ArchG133.24-00.04	02 18 20.1	+61 04 54	< 4.3	2.2	< 2	32.5	3.1	11	138	15	9	635	92	7
207	ArchG133.42+00.08	02 20 01.9	+61 08 07	7.6	2.5	3	36.4	3.6	10	147	20	7	707	78	9
208	ArchG133.69+01.21	02 25 26.1	+62 05 59	122.1	1.4	90	241.9	2.9	84	966	13	74	5638	49	114
209	ArchG134.41+00.26	02 28 14.2	+60 57 11	5.9	2.0	3	15.7	2.8	6	< 38	19	< 2	466	47	10
210	ArchG134.64+02.29	02 36 34.3	+62 44 29	4.5	1.7	3	16.4	3.0	6	76	24	3	297	51	6
211	ArchG135.09-00.07	02 32 22.0	+60 23 33	< 4.8	2.4	< 2	25.9	3.6	7	100	14	7	469	78	6
212	ArchG135.34+01.11*	02 38 03.5	+61 23 01	24.3	1.5	16	26.9	2.9	9	119	14	8	721	58	12
213	ArchG136.35+07.46	03 12 52.5	+66 34 43	< 2.2	1.1	< 2	10.8	1.9	6	< 25	12	< 2	190	28	7
214	ArchG136.58+01.11	02 47 24.0	+60 52 06	5.5	2.2	3	38.0	3.3	12	155	19	8	964	47	20
215	ArchG136.85+01.07	02 49 16.9	+60 42 57	23.0	1.2	19	68.6	2.2	31	254	15	16	1367	34	39
216	ArchG137.76+01.41	02 57 08.7	+60 36 28	11.4	1.5	8	34.4	2.1	16	197	10	18	708	58	12</

**Table 3.** continued.

N	Name	RA (2000)	Dec (2000)	$F_{143}$	$\sigma_{143}$	S/N	$F_{217}$	$\sigma_{217}$	S/N	$F_{353}$	$\sigma_{353}$	S/N	$F_{545}$	$\sigma_{545}$	S/N
220	ArchG140.61+00.67	03 13 49.5	+58 33 50	< 3.6	1.8	< 2	16.1	3.0	5	48	16	3	271	45	6
221	ArchG140.91-01.10	03 09 00.3	+56 53 33	10.6	2.2	5	48.8	3.8	13	177	24	7	958	67	14
222	ArchG140.91+05.81	03 39 21.1	+62 40 07	< 3.0	1.5	< 2	19.0	2.7	7	81	11	7	297	45	7
223	ArchG141.57-00.75*	03 14 29.8	+56 51 26	12.1	2.0	6	47.1	3.5	14	171	22	8	920	65	14
224	ArchG142.03+00.60	03 22 43.2	+57 45 04	5.2	1.8	3	22.9	3.3	7	103	17	6	449	45	10
225	ArchG142.11+01.77*	03 28 09.2	+58 40 50	12.5	1.8	7	60.7	4.1	15	244	16	15	1469	58	25
226	ArchG143.79-01.59	03 24 40.5	+54 57 25	< 4.4	2.2	< 2	26.4	3.4	8	108	18	6	430	78	6
227	ArchG146.24-00.54	03 42 41.6	+54 23 42	< 4.7	2.4	< 2	22.0	4.1	5	101	20	5	466	78	6
228	ArchG147.85+09.20	04 41 04.4	+60 24 59	< 3.2	1.6	< 2	16.1	2.5	6	72	12	6	293	47	6
229	ArchG148.02+00.18	03 55 14.2	+53 50 44	8.5	2.5	3	38.9	4.2	9	155	25	6	589	67	9
230	ArchG148.43-00.68	03 53 42.6	+52 55 23	< 4.2	2.1	< 2	13.6	3.8	4	83	16	5	281	51	5
231	ArchG148.79+02.18	04 08 14.4	+54 50 50	< 5.4	2.7	< 2	< 10.0	5.0	< 2	142	18	8	407	60	7
232	ArchG150.41+03.91	04 24 42.4	+54 58 30	< 5.0	2.5	< 2	20.2	4.1	5	123	23	5	543	95	6
233	ArchG150.63-00.87	04 03 48.2	+51 21 04	9.1	2.3	4	40.2	3.4	12	83	18	4	593	67	9
234	ArchG151.49-00.36*	04 10 04.3	+51 09 21	19.3	1.9	10	54.2	3.7	14	222	15	14	730	65	11
235	ArchG154.67+02.58	04 37 35.0	+50 57 02	11.6	1.7	7	37.8	3.9	10	172	23	7	699	53	13
236	ArchG157.06-02.82	04 23 50.0	+45 31 00	< 5.1	2.5	< 2	20.7	4.1	5	< 42	21	< 2	483	60	8
237	ArchG158.00-21.44	03 25 23.0	+30 45 13	6.8	2.4	3	23.0	4.4	5	< 40	20	< 2	348	67	5
238	ArchG158.34-20.53	03 29 07.0	+31 17 13	25.8	2.3	11	93.5	3.9	24	420	18	23	2046	92	22
239	ArchG159.17-34.44	02 56 01.1	+19 31 17	5.5	1.5	4	27.6	2.8	10	108	24	4	608	78	8
240	ArchG159.17-20.11	03 33 12.7	+31 09 03	8.8	3.2	3	52.3	4.4	12	205	21	10	1028	135	8
241	ArchG159.23-20.38*	03 32 38.2	+30 54 05	5.7	2.0	3	46.4	3.5	13	204	19	11	1087	75	14
242	ArchG159.75-19.41	03 37 14.0	+31 21 51	8.5	2.6	3	22.0	4.7	5	124	23	5	535	78	7
243	ArchG160.21-18.45	03 41 40.0	+31 49 51	< 5.4	2.7	< 2	35.4	4.6	8	162	28	6	0	-1	0
244	ArchG160.37-18.12*	03 43 11.2	+31 59 43	13.0	1.8	7	68.9	4.4	16	226	22	10	1458	46	32
245	ArchG160.57-16.79	03 47 56.6	+32 52 59	< 4.8	2.4	< 2	23.7	5.2	5	149	28	5	546	95	6
246	ArchG165.24-09.00	04 29 52.5	+35 21 47	12.7	2.0	6	51.8	4.2	12	301	16	19	1376	58	24
247	ArchG168.10-16.35	04 13 49.6	+28 16 44	8.1	2.3	4	23.2	4.4	5	115	28	4	714	95	7
248	ArchG168.79-15.63	04 18 17.4	+28 17 54	13.2	2.3	6	46.0	3.5	13	180	18	10	1117	92	12
249	ArchG169.80-16.22	04 19 20.5	+27 11 27	7.1	2.7	3	19.4	3.7	5	58	14	4	379	67	6
250	ArchG172.01-16.97	04 23 17.6	+25 07 08	< 4.0	2.0	< 2	18.8	3.6	5	68	16	4	571	60	9
251	ArchG173.35+02.27	05 38 07.4	+35 46 56	14.8	2.1	7	51.8	4.3	12	179	19	9	795	65	12
252	ArchG173.38-16.32*	04 29 15.3	+24 34 14	7.8	1.8	4	36.8	3.3	11	192	14	13	749	65	11
253	ArchG173.52-01.75	05 22 16.3	+33 25 41	7.8	2.3	3	29.6	4.4	7	68	28	2	501	67	7
254	ArchG173.62+02.77*	05 40 56.8	+35 49 19	23.0	2.0	11	121.0	3.6	34	441	23	18	2176	92	24
255	ArchG173.96-15.89	04 32 17.9	+24 25 32	5.8	2.9	2	29.5	4.5	7	105	23	4	418	78	5
256	ArchG174.05-13.79	04 39 38.0	+25 42 41	< 6.0	3.0	< 2	38.5	4.4	9	183	13	13	916	92	10
257	ArchG174.71-15.42	04 35 52.9	+24 10 43	< 4.8	2.4	< 2	18.7	4.5	4	114	20	6	458	60	8
258	ArchG175.24-12.27	04 48 06.5	+25 46 38	4.8	1.8	3	16.9	3.3	5	71	28	2	414	42	10
259	ArchG175.61-16.76	04 33 50.6	+22 39 09	< 5.0	2.5	< 2	12.8	4.9	3	104	18	6	360	67	5
260	ArchG176.61-01.76	05 30 22.5	+30 51 34	5.6	2.4	2	20.6	3.8	5	114	21	5	299	95	3
261	ArchG177.50-20.29	04 27 11.4	+19 00 50	3.1	0.9	3	23.0	1.8	13	165	10	16	404	29	14
262	ArchG178.85-20.09	04 31 14.1	+18 09 34	10.3	1.0	10	38.9	1.7	23	137	13	10	791	32	24
263	ArchG180.63-19.47	04 37 37.6	+17 14 32	3.0	0.9	3	8.3	1.7	5	< 20	10	< 2	181	24	7
264	ArchG180.78+04.20	06 04 06.3	+30 23 00	< 5.1	2.5	< 2	18.3	4.3	4	152	24	6	635	67	9
265	ArchG182.02+00.36	05 51 44.9	+27 23 15	< 5.0	2.5	< 2	10.4	4.4	2	89	17	5	361	67	5
266	ArchG182.09-00.50	05 48 34.6	+26 53 25	4.3	1.8	2	22.3	3.2	7	78	18	4	466	67	7
267	ArchG182.17-17.89	04 46 37.3	+17 02 48	2.6	1.3	2	21.7	1.8	12	73	7	10	256	55	5
268	ArchG182.44+00.25	05 52 17.2	+26 58 17	< 3.9	1.9	< 2	22.5	3.6	6	110	14	8	217	67	3
269	ArchG183.21-00.65	05 50 34.6	+25 51 11	7.0	1.6	4	23.9	2.4	10	86	14	6	347	60	6
270	ArchG183.63-03.74	05 39 55.6	+23 53 23	5.8	1.8	3	20.8	3.3	6	64	14	5	385	45	9
271	ArchG184.55-05.77	05 34 33.9	+22 01 29	231.4	1.4	165	181.9	1.8	101	185	11	16	236	58	4
272	ArchG184.58-04.14	05 40 36.1	+22 51 59	3.7	1.5	2	15.5	2.9	5	68	15	4	375	42	9
273	ArchG185.56-02.39	05 49 20.0	+22 56 37	< 2.9	1.4	< 2	21.1	3.0	7	53	11	5	397	37	11
274	ArchG186.43-05.43	05 40 04.6	+20 37 33	3.5	1.5	2	13.3	2.6	5	26	12	2	223	39	6
275	ArchG186.76-05.35	05 41 06.0	+20 22 48	5.0	1.5	3	15.1	2.8	5	< 44	22	< 2	278	51	5
276	ArchG188.43+02.96	06 15 40.3	+23 05 24	< 3.6	1.8	< 2	14.8	2.6	6	65	9	7	246	60	4
277	ArchG188.51+03.59	06 18 16.7	+23 19 13	5.6	1.8	3	21.3	2.6	8	101	9	10	490	55	9
278	ArchG188.86+01.12*	06 09 35.8	+21 49 36	16.9	1.5	12	71.2	2.0	36	255	9	27	1305	58	22
279	ArchG188.93+04.46	06 22 28.9	+23 21 18	4.5	1.5	3	19.4	3.1	6	108	18	6	345	40	8
280	ArchG189.30+05.82	06 28 29.4	+23 39 15	30.7	2.8	11	92.5	5.5	17	441	37	12	0	-1	0
281	ArchG189.41-10.17	05 29 41.3	+15 36 40	< 1.6	0.8	< 2	7.2	1.3	5	25	9	3	138	21	7
282	ArchG189.41+04.32	06 22 53.7	+22 51 47	16.1	1.4	11	53.3	2.3	23	122	8	15	548	53	10
283	ArchG189.69+05.44	06 27 46.0	+23 08 01	27.0	4.5	6	124.0	6.5	19	0	-1	0	0	-1	0
284	ArchG189.77+00.73	06 10 00.2	+20 50 36	< 2.7	1.4	< 2	19.1	2.5	8	82	13	6	387	45	9
285	ArchG189.86+00.37	06 08 50.7	+20 35 26	31.2	1.4	23	143.1	2.1	68	556	12	45	3127	53	59
286	ArchG190.05+00.64	06 10 14.9	+20 33 33	9.9	1.6	6	42.7	2.8	15	162	11	14	0	-1	0
287	ArchG190.39-02.09	06 00 50.7	+18 55 33	3.4	1.3	3	13.6	2.4	6	70	17	4	301	30	10
288	ArchG190.57+00.76	06 11 47.4	+20 09 30	< 3.0	1.5	< 2	17.2	2.4	7	75	12	6	425	45	9
289	ArchG191.64-00.84	06 08 01.0	+18 26 51	< 2.7	1.3	< 2	14.9	2.2	7	35	17	2	308	60	5
290	ArchG191.86+00.88	06 14 49.3	+19 05 00	3.3	1.5	2	17.3	2.6	7	69	11	6	328	55	6
291	ArchG192.04-02.72	06 01 58.5	+17 10 51	< 2.4	1.2	< 2	10.5	2.1	5						

**Table 3.** continued.

N	Name	RA (2000)	Dec (2000)	$F_{143}$	$\sigma_{143}$	S/N	$F_{217}$	$\sigma_{217}$	S/N	$F_{353}$	$\sigma_{353}$	S/N	$F_{545}$	$\sigma_{545}$	S/N
295	ArchG192.65–03.78	05 59 21.8	+16 07 22	2.6	0.9	3	10.9	1.7	6	50	6	8	314	36	9
296	ArchG193.96–02.54	06 06 32.4	+15 35 45	< 2.2	1.1	< 2	7.3	1.4	5	42	4	9	146	29	5
297	ArchG194.01–00.43	06 14 20.7	+16 34 05	2.5	1.2	2	16.3	2.2	7	53	13	4	247	39	6
298	ArchG194.41–00.92	06 13 18.8	+15 59 06	2.1	0.9	2	13.2	1.3	10	63	6	11	225	29	8
299	ArchG194.73–03.49	06 04 39.8	+14 27 34	4.0	1.5	3	17.4	2.6	7	0	-1	0	481	47	10
300	ArchG194.83–01.17	06 13 14.1	+15 29 41	1.6	0.7	2	13.2	1.1	12	53	3	14	178	30	6
301	ArchG195.64–00.08	06 18 49.6	+15 18 16	3.8	0.9	4	15.5	1.6	10	79	10	8	327	25	13
302	ArchG195.73–02.39	06 10 36.3	+14 07 21	6.8	1.1	6	19.5	1.6	12	0	-1	0	0	-1	0

**Table 4.** Model fit parameters and associations. For each point source, the emissivity exponent  $\beta$  and temperature  $T$  are given along with the reduced  $\chi^2$  value. When the fit is unsatisfactory (see Sect. 3.3),  $\beta_{11}$  (assuming a fixed temperature of 11 K), or  $T_2$  (assuming a fixed exponent index of 2) are provided instead. The associated IRAS source is given along with the far infrared fluxes. A star by the name of the IRAS counterpart indicates that the IRAS source has the (IRAS) colors of an ultra-compact HII region. Then associations with a commonly used name are given with Lynds Dark Nebulae, Bright Nebulae, Sharpless and other common catalogs. Associations with HII regions (with angular size  $\leq 10$  arcmin) from the catalogue by Paladini et al. (2003) are also given.

N	Name	$\beta$	T (K)	$\chi^2_r$	$\beta_{11}$	$T_2$ (K)	Iras Name	$F_\nu(100\mu\text{m})/\text{Jy}$	$F_\nu(60\mu\text{m})/\text{Jy}$	Common Name A
1	ArchG063.36+11.11	$1.60 \pm 0.50$	$10.50 \pm 1.05$	1.31	$2.24 \pm 0.04$	$11.60 \pm 0.10$	19040+3157	7.3	0.4	-
2	ArchG073.55+02.63				$3.72 \pm 0.02$	$18.40 \pm 0.15$	20042+3643	72.5	6.7	-
3	ArchG075.75+00.33				$1.72 \pm 0.02$	$10.30 \pm 0.10$	X2019+373	21000.0	18000.0	MWC1015 G075.
4	ArchG075.97+00.69						20187+3738	94.3	16.0	-
5	ArchG076.81+02.14	$1.10 \pm 0.23$	$21.90 \pm 2.50$	5.70	$3.26 \pm 0.02$	$14.20 \pm 0.10$	20158+3913	1610.0	556.0	RAFGL 2549
6	ArchG077.35+01.83				$2.58 \pm 0.04$	$12.50 \pm 0.10$	20188+3928 *	1440.0	1050.0	-
7	ArchG077.59+00.62				$3.12 \pm 0.02$	$13.90 \pm 0.10$	20243+3853 *	226.0	109.0	-
8	ArchG077.88+01.78				$3.64 \pm 0.03$	$16.10 \pm 0.10$	20205+3948 *	1340.0	788.0	-
9	ArchG077.95–00.14				$3.40 \pm 0.03$	$16.30 \pm 0.20$	20277+3851 *	3100.0	1870.0	DR 9
10	ArchG078.11–00.50						20304+3839 *	4920.0	1400.0	RAFGL 4267
11	ArchG078.17+03.95	$0.98 \pm 0.37$	$16.70 \pm 2.15$	3.10	$3.04 \pm 0.02$	$14.00 \pm 0.10$	20117+4123	153.0	13.8	V 431 CYG
12	ArchG078.50+01.05				$3.02 \pm 0.02$	$13.70 \pm 0.10$	20256+3951	1760.0	185.0	DR 5 W 67
13	ArchG079.15+02.22						20216+4107 *	718.0	295.0	-
14	ArchG079.22+00.28	$2.08 \pm 0.08$	$17.80 \pm 0.50$	0.87			20306+4005 *	10100.0	7720.0	RAFGL 2602 G0
15	ArchG079.37+00.94	$3.96 \pm 0.17$	$8.70 \pm 0.10$	0.20			20281+4038	304.0	123.0	-
16	ArchG079.37+01.20				$3.94 \pm 0.02$	$17.00 \pm 0.10$	20264+4042 *	4600.0	2330.0	RAFGL 2586 DR
17	ArchG079.43+03.37	$2.04 \pm 0.22$	$12.10 \pm 0.50$	1.11			20178+4157	272.0	9.4	-
18	ArchG079.57+03.57				$2.86 \pm 0.04$	$13.30 \pm 0.10$	20172+4206	235.0	30.0	-
19	ArchG079.69+01.12				$2.30 \pm 0.02$	$11.70 \pm 0.10$	20285+4049	190.0	44.3	DR 11
20	ArchG079.90+02.54				$2.70 \pm 0.02$	$13.00 \pm 0.10$	20227+4156	463.0	25.6	LDN 0897
21	ArchG080.51+03.32	$1.40 \pm 0.41$	$16.40 \pm 2.40$	2.86	$3.68 \pm 0.02$	$16.10 \pm 0.10$	20212+4259	254.0	23.4	MRSL 080+03/4
22	ArchG080.89+00.30				$2.46 \pm 0.02$	$12.30 \pm 0.10$	20350+4126 *	3270.0	1300.0	RAFGL 2616 G0
23	ArchG080.91–00.14				$0.90 \pm 0.03$	$8.30 \pm 0.10$	20373+4108	538.0	147.0	G080.9+00.4–HII
24	ArchG081.24+00.57				$1.84 \pm 0.02$	$10.60 \pm 0.10$	20325+4211	100.0	14.0	-
25	ArchG081.26+01.12				$3.04 \pm 0.05$	$13.90 \pm 0.10$	20261+4339	300.0	15.3	-
26	ArchG081.59+03.03				$0.84 \pm 0.02$	$8.20 \pm 0.10$				DR 21 G081.7+00
27	ArchG081.67+00.53				$2.74 \pm 0.02$	$12.80 \pm 0.10$	X2027+433	469.0	0.0	-
28	ArchG081.68+02.76				$0.96 \pm 0.02$	$8.30 \pm 0.10$				G082.0+02.3–HII
29	ArchG081.94+02.31				$0.82 \pm 0.13$	$8.00 \pm 0.50$				-
30	ArchG082.48+00.16									-
31	ArchG082.93+03.38				$0.80 \pm 0.14$	$7.90 \pm 0.55$				-
32	ArchG083.04+01.93				$1.04 \pm 0.07$	$8.50 \pm 0.15$				-
33	ArchG083.61–02.12				$0.98 \pm 0.05$	$8.30 \pm 0.10$				-
34	ArchG083.75+03.31				$0.90 \pm 0.04$	$8.20 \pm 0.15$				LBN 083.77+03.3
35	ArchG084.64+00.18	$1.66 \pm 0.06$	$16.20 \pm 0.35$	2.08	$1.06 \pm 0.02$	$8.50 \pm 0.10$	X2048+441	1480.0	0.0	-
36	ArchG084.79–01.15									G084.9–01.2–HII
37	ArchG084.82+01.59	$2.04 \pm 0.33$	$11.80 \pm 0.85$	1.92			X2044+453	83.6	0.0	-
38	ArchG084.84+03.86	$1.84 \pm 0.13$	$14.10 \pm 0.45$	4.94			20334+4636	408.0	3.0	S 115
39	ArchG084.96–00.39				$1.00 \pm 0.03$	$8.40 \pm 0.10$				-
40	ArchG085.14+03.94				$2.52 \pm 0.02$	$12.30 \pm 0.10$	20334+4649	158.0	36.3	-
41	ArchG085.45+02.73	$3.34 \pm 0.29$	$8.20 \pm 0.30$	1.50	$1.02 \pm 0.10$	$8.20 \pm 0.45$	20406+4628	15.5	1.8	-
42	ArchG086.41+00.44				$0.90 \pm 0.12$	$7.20 \pm 0.75$				-
43	ArchG086.65+00.38				$1.68 \pm 0.04$	$10.20 \pm 0.10$	20333+4902	13.4	1.1	DO 38622
44	ArchG086.72+05.30						20413+4841	38.0	1.3	-
45	ArchG087.30+04.05	$2.80 \pm 0.53$	$9.90 \pm 0.90$	0.36	$1.82 \pm 0.03$	$10.60 \pm 0.10$	21072+4726	23.2	0.9	-
46	ArchG089.30–00.04						20597+4911	38.8	3.0	LDN 0978
47	ArchG089.57+02.09	$1.40 \pm 0.45$	$12.70 \pm 1.65$	1.73			21183+4645	19.4	0.7	-
48	ArchG089.93–01.97	$3.54 \pm 0.25$	$7.90 \pm 0.25$	3.73			21023+5002	199.0	86.9	LDN 0988
49	ArchG090.39+02.32	$2.98 \pm 0.19$	$10.30 \pm 0.30$	5.68	$3.44 \pm 0.02$	$15.10 \pm 0.10$	21074+4949 *	715.0	344.0	-
50	ArchG090.97+01.49									-
51	ArchG091.10+01.77	$2.50 \pm 0.41$	$10.60 \pm 0.85$	2.24	$2.12 \pm 0.03$	$11.30 \pm 0.10$	21066+5009	52.6	8.1	-
52	ArchG091.32–00.30				$1.24 \pm 0.02$	$9.30 \pm 0.10$	X2116+488	46.3	11.3	-
53	ArchG092.03+03.93						21005+5217	11.0	7.5	LDN 1004
54	ArchG092.22+02.85	$2.70 \pm 0.30$	$9.90 \pm 0.50$	2.44			21065+5134	47.5	3.7	-
55	ArchG092.57+04.61	$3.98 \pm 0.28$	$7.30 \pm 0.10$	1.48			21001+5311	8.4	0.6	-
56	ArchG092.90+04.05				$1.80 \pm 0.04$	$10.50 \pm 0.10$	21045+5252	16.8	3.6	-
57	ArchG093.10+02.79	$0.68 \pm 0.10$	$25.70 \pm 1.65$	2.01			21108+5220 *	912.0	176.0	G093.1+02.8–HII
58	ArchG093.40–00.15	$2.02 \pm 0.31$	$11.90 \pm 0.75$	2.24			21261+5018	71.5	5.5	-
59	ArchG093.78+01.91	$1.62 \pm 0.26$	$13.20 \pm 0.85$	0.30			21191+5212	81.6	30.5	-
60	ArchG094.01+09.86				$1.32 \pm 0.06$	$9.40 \pm 0.10$	20379+5729	3.2	0.6	-
61	ArchG094.38–05.46	$2.42 \pm 0.22$	$13.00 \pm 0.70$	1.70			21514+4705	774.0	149.0	S 125 LDN 1055
62	ArchG094.56–00.06	$2.42 \pm 0.39$	$11.60 \pm 0.95$	3.87			21301+5112	120.0	2.1	-
63	ArchG095.62–00.76	$4.00 \pm 0.38$	$8.30 \pm 0.20$	1.46			X2139+514A	56.1	25.3	RAFGL 2791S
64	ArchG096.05+08.02	$2.82 \pm 0.38$	$8.40 \pm 0.45$	0.23			20586+5802	5.3	0.9	-

**Table 4.** continued.

N	Name	$\beta$	T (K)	$\chi^2_r$	$\beta_{11}$	$T_2$ (K)	Iras Name	$F_\nu(100\mu\text{m})/\text{Jy}$	$F_\nu(60\mu\text{m})/\text{Jy}$	Common Name A
65	ArchG096.26-00.14	$1.48 \pm 0.28$	$12.80 \pm 0.90$	3.69			21391+5227	38.6	5.8	-
66	ArchG097.32+09.90	$3.02 \pm 0.38$	$8.20 \pm 0.40$	2.21			20520+6003	6.3	2.5	-
67	ArchG097.44+03.25				$3.26 \pm 0.02$	$14.50 \pm 0.10$	21306+5540 *	958.0	714.6	G097.5+03.2-HII
68	ArchG097.68+03.18				$2.96 \pm 0.02$	$13.70 \pm 0.10$	21306+5540 *	958.0	715.0	G097.6+03.2-HII
69	ArchG097.82+08.67	$2.44 \pm 0.38$	$9.50 \pm 0.55$	0.99			21034+5941	11.5	3.2	-
70	ArchG098.00+01.55				$3.56 \pm 0.02$	$15.40 \pm 0.10$	21407+5441 *	1270.0	246.0	LDN 1084
71	ArchG098.35+06.11				$2.40 \pm 0.04$	$12.00 \pm 0.10$	21197+5825	47.6	1.3	-
72	ArchG098.43+13.79				$1.50 \pm 0.04$	$9.90 \pm 0.10$	20319+6330	6.0	2.1	-
73	ArchG099.11+00.69	$3.14 \pm 0.42$	$8.90 \pm 0.50$	5.26			21500+5451	24.4	1.1	TMSS +50403
74	ArchG099.13+01.00				$2.22 \pm 0.05$	$11.50 \pm 0.10$	21481+5505	32.3	0.5	-
75	ArchG099.37+01.27				$1.06 \pm 0.13$	$8.40 \pm 0.50$				-
76	ArchG100.01+04.26	$2.22 \pm 0.16$	$13.40 \pm 0.50$	1.00			21391+5802 *	425.0	145.0	LDN 1121
77	ArchG100.16+03.02				$2.72 \pm 0.05$	$12.80 \pm 0.10$	21451+5713	86.8	2.9	-
78	ArchG100.22+02.06	$1.58 \pm 0.35$	$19.10 \pm 2.55$	1.01			21503+5631 *	567.0	266.0	-
79	ArchG100.35+03.35	$3.28 \pm 0.25$	$9.20 \pm 0.30$	0.23			21449+5737	67.3	8.9	LDN 1129
80	ArchG100.44+08.84				$2.44 \pm 0.03$	$12.10 \pm 0.10$	21161+6141	53.4	12.3	-
81	ArchG100.57+16.40				$1.40 \pm 0.06$	$9.70 \pm 0.10$	20223+6622	2.6	0.4	-
82	ArchG101.41+02.59				$2.88 \pm 0.04$	$13.30 \pm 0.10$	X2154+576	149.0	74.5	BFS10 G101.5+0
83	ArchG101.63+11.17				$1.14 \pm 0.13$	$8.60 \pm 0.50$				-
84	ArchG101.96-00.21	$2.00 \pm 0.34$	$11.30 \pm 0.80$	2.17			22101+5544	35.3	2.2	-
85	ArchG102.08+11.11				$1.42 \pm 0.13$	$9.10 \pm 0.35$				-
86	ArchG102.16+15.35				$0.86 \pm 0.05$	$8.90 \pm 0.10$	20395+6714	2.8	0.4	LDN 1147
87	ArchG102.35+08.32	$2.54 \pm 0.40$	$9.70 \pm 0.65$	1.69			21309+6245	13.8	0.4	-
88	ArchG102.69+08.43				$1.14 \pm 0.10$	$8.60 \pm 0.35$				-
89	ArchG102.71-00.78	$2.02 \pm 0.17$	$13.10 \pm 0.50$	2.29			X2216+556	306.0	0.0	S 132
90	ArchG102.80+02.13	$3.08 \pm 0.32$	$9.80 \pm 0.50$	3.25			X2206+582	77.4	13.2	LDN 1159
91	ArchG103.43+13.69				$0.82 \pm 0.18$	$5.40 \pm 0.90$				-
92	ArchG103.73+02.18	$1.80 \pm 0.15$	$18.70 \pm 1.00$	1.15			X2211+587	2050.0	953.0	G103.7+02.2-HII
93	ArchG103.97+10.93	$2.06 \pm 0.22$	$12.10 \pm 0.60$	1.49			X2124+656	56.9	0.0	-
94	ArchG104.10+12.23				$1.72 \pm 0.26$	$16.00 \pm 1.40$	4.47			-
95	ArchG104.49+01.33				$2.44 \pm 0.02$	$12.10 \pm 0.10$	22196+5830	493.0	63.1	S 135
96	ArchG104.66+11.38				$1.24 \pm 0.08$	$8.90 \pm 0.25$				-
97	ArchG104.69+00.30	$1.82 \pm 0.36$	$14.50 \pm 1.50$	0.18			22246+5750	196.0	93.0	-
98	ArchG104.77+02.88	$2.26 \pm 0.33$	$14.00 \pm 1.20$	0.42			X2214+598	429.0	365.0	-
99	ArchG104.99+07.26	$2.52 \pm 0.40$	$10.60 \pm 0.75$	2.41			21540+6341	30.5	0.9	OCL 0239
100	ArchG105.39+09.89	$1.64 \pm 0.06$	$19.30 \pm 0.45$	4.97			X2141+658	1980.0	1150.0	LDN 1183 BFS1
101	ArchG105.55+10.45				$2.02 \pm 0.02$	$11.00 \pm 0.10$	21381+6630	23.8	0.4	-
102	ArchG105.69+00.44	$1.88 \pm 0.24$	$15.40 \pm 1.05$	0.76			22308+5812 *	1038.0	873.7	S138 G105.6+00.
103	ArchG105.74+01.35				$2.18 \pm 0.03$	$11.40 \pm 0.10$	22286+5905	36.5	3.0	-
104	ArchG105.89+04.17				$2.44 \pm 0.02$	$12.10 \pm 0.10$	22161+6140	90.9	32.8	-
105	ArchG106.52+07.09	$2.74 \pm 0.44$	$9.70 \pm 0.70$	0.55			22051+6425	16.6	1.3	-
106	ArchG106.53+01.11	$2.86 \pm 0.23$	$9.20 \pm 0.30$	1.20			22334+5922	41.5	2.7	-
107	ArchG106.88+05.29				$2.36 \pm 0.02$	$11.90 \pm 0.10$	22176+6303 *	13460.0	11230.0	S140 RAFGL 288
108	ArchG107.17-00.91				$3.72 \pm 0.02$	$16.10 \pm 0.10$	22457+5751	1090.0	431.0	S 142 G107.2-01.
109	ArchG107.22+00.04	$1.50 \pm 0.34$	$13.30 \pm 1.20$	0.32			22437+5841	51.0	3.9	-
110	ArchG107.37+07.65	$2.86 \pm 0.31$	$9.10 \pm 0.40$	1.96			22103+6523	12.6	0.9	-
111	ArchG108.11+02.75	$2.80 \pm 0.19$	$9.80 \pm 0.30$	5.21			X2237+614	62.4	27.0	-
112	ArchG108.15+05.52	$1.96 \pm 0.33$	$17.60 \pm 1.85$	0.50			22272+6358A *	727.0	378.0	LDN 1206 G108.
113	ArchG108.23-01.19	$2.24 \pm 0.41$	$16.00 \pm 1.95$	0.12			22535+5813	861.0	29.0	S 147
114	ArchG108.34+00.52	$1.20 \pm 0.24$	$24.10 \pm 3.05$	1.76			X2247+596	1070.0	827.0	S 146 G108.2+00.
115	ArchG108.63+00.45				$2.84 \pm 0.02$	$13.30 \pm 0.10$	22506+5944 *	295.0	188.0	-
116	ArchG108.80+01.40	$1.86 \pm 0.27$	$11.70 \pm 0.70$	1.53			22490+6043	39.5	5.3	-
117	ArchG108.85-01.05	$1.56 \pm 0.12$	$21.60 \pm 1.25$	2.42			X2256+585	3660.0	2220.0	S 152 G108.8-01.
118	ArchG108.89+02.69	$2.16 \pm 0.12$	$15.60 \pm 0.55$	3.07			X2245+618	1550.0	652.0	LDN 1211 G109.
119	ArchG109.01-00.36				$3.56 \pm 0.02$	$15.30 \pm 0.10$	22570+5912 *	962.0	692.0	-
120	ArchG109.43+06.56				$1.84 \pm 0.02$	$10.60 \pm 0.10$	22313+6525	60.5	8.4	LDN 1214
121	ArchG109.51+08.77				$1.58 \pm 0.04$	$10.20 \pm 0.10$	22226+6726	5.4	0.6	-
122	ArchG109.80+08.63				$1.40 \pm 0.05$	$9.90 \pm 0.10$	22233+6734	3.3	0.5	-
123	ArchG109.82+02.17				$4.00 \pm 0.02$	$21.50 \pm 0.10$	22543+6145 *	20500.0	12800.0	RAFGL 2997S
124	ArchG109.89+05.34	$3.24 \pm 0.25$	$8.30 \pm 0.25$	0.83			22405+6436	7.5	0.7	-
125	ArchG110.26+02.46				$4.00 \pm 0.02$	$17.50 \pm 0.10$	22551+6221	3010.0	1630.0	S 155 G110.2+02
126	ArchG110.50-00.42				$1.94 \pm 0.02$	$10.90 \pm 0.10$	23077+5941	85.5	4.4	-
127	ArchG110.75+05.30	$1.40 \pm 0.64$	$12.20 \pm 2.15$	5.79			22496+6458	8.5	1.4	-
128	ArchG110.80+06.56				$1.24 \pm 0.14$	$8.70 \pm 0.60$				-
129	ArchG110.87-02.84				$1.70 \pm 0.03$	$10.30 \pm 0.10$	23162+5732	17.8	4.7	-
130	ArchG110.88-01.21	$1.74 \pm 0.31$	$13.50 \pm 1.10$	2.00			23121+5914	121.0	37.0	-
131	ArchG110.93+03.79				$1.94 \pm 0.03$	$10.90 \pm 0.10$	22575+6337	14.8	0.9	-
132	ArchG111.11-03.01	$3.10 \pm 0.35$	$8.60 \pm 0.40$	0.19			23191+5730	23.3	1.0	-
133	ArchG111.29-00.68	$1.62 \pm 0.06$	$17.70 \pm 0.40$	4.76			23138+5945 *	2160.0	1770.0	S 157 RAFGL 30
134	ArchG111.42-02.91				$2.06 \pm 0.02$	$11.10 \pm 0.10$	X2321+575	70.4	0.0	-
135	ArchG111.53+00.75				$3.94 \pm 0.02$	$16.70 \pm 0.10$	23116+6111 *	14100.0	7070.0	S 158 RAFGL 30
136	ArchG111.70-02.13				$1.56 \pm 0.02$	$10.30 \pm 0.10$	23210+5837	54.0	2.8	CAS A W 81 SNI
137	ArchG111.87+05.99	$2.78 \pm 0.45$	$9.30 \pm 0.70$	4.80			22542+6607	9.2	0.6	-
138	ArchG112.05+01.66	$2.92 \pm 0.37$	$9.80 \pm 0.55$	2.49			23123+6203	41.1	2.3	-
139	ArchG112.20+05.26	$3.12 \pm 0.41$	$9.20 \pm 0.55$	0.92			23011+6534	21.6	0.8	-

**Table 4.** continued.

N	Name	$\beta$	T (K)	$\chi^2_r$	$\beta_{11}$	$T_2$ (K)	Iras Name	$F_\nu(100\mu\text{m})/\text{Jy}$	$F_\nu(60\mu\text{m})/\text{Jy}$	Common Name A
140	ArchG112.43+02.84				$2.04 \pm 0.02$	$11.10 \pm 0.10$	23126+6317	42.1	1.1	-
141	ArchG112.76-02.05	$2.34 \pm 0.39$	$10.10 \pm 0.70$	1.52	$2.20 \pm 0.04$	$11.50 \pm 0.10$	23289+5852	20.5	0.9	-
142	ArchG113.36+06.93	$3.92 \pm 0.40$	$8.20 \pm 0.30$	0.43	$3.32 \pm 0.02$	$14.70 \pm 0.10$	23054+6732	15.7	0.5	-
143	ArchG113.39+01.54						23246+6231	29.7	4.4	-
144	ArchG113.58-00.70						23306+6031	719.0	88.8	S163 LDN 1245
145	ArchG113.61+01.77	$2.52 \pm 0.42$	$10.90 \pm 0.85$	0.46			X2324+629	40.9	0.0	-
146	ArchG114.07+02.01	$2.28 \pm 0.34$	$10.40 \pm 0.65$	6.14			23275+6308	21.0	1.1	-
147	ArchG114.17+06.69				$1.70 \pm 0.04$	$10.40 \pm 0.10$	23153+6738	8.0	0.6	-
148	ArchG114.28+05.95				$1.36 \pm 0.02$	$9.70 \pm 0.10$	23184+6652	5.3	0.5	-
149	ArchG114.31+06.18				$1.36 \pm 0.02$	$9.60 \pm 0.10$	23185+6715	4.8	1.0	-
150	ArchG114.33+03.28	$3.26 \pm 0.46$	$10.10 \pm 0.80$	0.15			X2328+643	81.2	22.5	-
151	ArchG114.38+01.07	$3.20 \pm 0.40$	$8.30 \pm 0.45$	0.27			23338+6232	9.9	1.9	-
152	ArchG114.52-00.47	$1.76 \pm 0.17$	$16.80 \pm 0.95$	0.78			23380+6057	938.0	2.8	-
153	ArchG115.15+05.30				$1.62 \pm 0.02$	$10.00 \pm 0.10$	23283+6642	6.6	0.5	-
154	ArchG115.24+02.54				$2.08 \pm 0.02$	$11.20 \pm 0.10$	X2336+639	31.3	0.0	-
155	ArchG115.24-01.46	$2.24 \pm 0.21$	$13.80 \pm 0.65$	2.00			X2344+601	560.0	240.0	-
156	ArchG115.47+05.75				$1.10 \pm 0.28$	$8.60 \pm 0.95$				-
157	ArchG115.83+03.97	$1.78 \pm 0.19$	$12.90 \pm 0.60$	3.05			X2339+656	70.7	20.9	-
158	ArchG115.83-03.06	$3.08 \pm 0.46$	$8.70 \pm 0.55$	2.33			23525+5844	21.1	1.2	LDN 1254
159	ArchG115.86+06.18				$1.48 \pm 0.02$	$9.90 \pm 0.10$	23325+6739	9.3	1.0	-
160	ArchG115.92-01.62	$2.14 \pm 0.16$	$13.00 \pm 0.45$	6.19			23504+6012	400.0	157.0	S 168/169 G115.8
161	ArchG117.33+03.14				$3.52 \pm 0.02$	$15.40 \pm 0.10$	23545+6508 *	1060.0	756.0	RAFGL 5623
162	ArchG117.55+02.25	$2.24 \pm 0.32$	$12.30 \pm 0.90$	1.54			23589+6421	102.0	6.4	S 170 G117.6+02.2
163	ArchG117.75-03.52	$1.92 \pm 0.38$	$14.90 \pm 1.55$	0.97			X0008+585	340.0	219.0	-
164	ArchG117.81+04.05	$1.68 \pm 0.12$	$15.30 \pm 0.55$	2.60			X2356+661	274.0	128.0	-
165	ArchG118.05+04.95				$3.02 \pm 0.02$	$14.10 \pm 0.10$	23572+6702	1140.0	105.0	LDN 1268 G118.
166	ArchG118.81+03.06	$1.96 \pm 0.18$	$13.90 \pm 0.65$	1.13			00082+6511	247.0	108.0	-
167	ArchG119.06+01.50				$1.16 \pm 0.14$	$8.70 \pm 0.50$				-
168	ArchG119.26-01.05	$1.38 \pm 0.27$	$12.20 \pm 0.80$	0.25			00179+6121	23.9	5.9	-
169	ArchG119.46-01.52	$2.88 \pm 0.30$	$9.30 \pm 0.40$	0.52			00198+6054	30.4	1.9	-
170	ArchG119.61+05.25				$2.36 \pm 0.04$	$11.90 \pm 0.10$	00130+6733	31.8	1.3	-
171	ArchG119.81+03.88	$2.72 \pm 0.29$	$9.90 \pm 0.45$	3.35			00165+6617	23.1	0.5	-
172	ArchG120.31+02.99				$1.54 \pm 0.02$	$9.90 \pm 0.10$	00227+6534	16.8	1.9	-
173	ArchG120.40+01.99	$3.08 \pm 0.42$	$12.90 \pm 1.10$	0.30			X0024+644	709.0	390.0	S 175 G120.4+02.9
174	ArchG120.67+04.02	$2.46 \pm 0.25$	$10.10 \pm 0.40$	4.99			00255+6621	20.8	2.1	-
175	ArchG120.67+01.20	$2.62 \pm 0.27$	$9.60 \pm 0.40$	1.69			00272+6350	25.0	2.0	-
176	ArchG120.92+02.89	$2.88 \pm 0.45$	$9.40 \pm 0.65$	3.01			00284+6518	18.4	0.9	-
177	ArchG121.07+01.16				$1.16 \pm 0.12$	$8.60 \pm 0.40$				-
178	ArchG121.29+03.19				$2.20 \pm 0.04$	$11.50 \pm 0.10$	X0033+657	22.1	6.1	LDN 1288
179	ArchG121.76+03.99	$1.56 \pm 0.28$	$20.40 \pm 2.40$	0.15			X0036+666	620.0	176.0	-
180	ArchG121.76+00.22	$2.08 \pm 0.32$	$10.80 \pm 0.70$	1.45			00379+6248	27.0	9.9	-
181	ArchG121.91-01.45	$2.62 \pm 0.48$	$9.50 \pm 0.75$	1.83			00401+6113	19.7	1.6	-
182	ArchG122.10+03.41				$1.22 \pm 0.11$	$8.90 \pm 0.30$				-
183	ArchG123.01-00.89				$2.38 \pm 0.02$	$12.00 \pm 0.10$	X0049+616	88.0	0.0	-
184	ArchG123.15-06.29				$3.50 \pm 0.02$	$15.30 \pm 0.10$	00494+5617 *	1170.0	330.0	S 184 G123.2-06.2
185	ArchG123.31+02.97	$2.14 \pm 0.28$	$14.50 \pm 1.05$	2.60			X0051+656	378.0	0.0	S 183
186	ArchG123.81+02.39	$2.04 \pm 0.29$	$10.10 \pm 0.55$	2.82			00578+6452	9.6	1.6	-
187	ArchG124.06+03.41				$1.28 \pm 0.05$	$8.80 \pm 0.15$	01031+6444	9.5	0.8	-
188	ArchG124.54+02.09	$3.34 \pm 0.22$	$7.70 \pm 0.20$	1.49			01045+6505 *	331.0	293.0	LDN 1307
189	ArchG124.61+02.37	$2.18 \pm 0.12$	$13.10 \pm 0.35$	1.95			01153+6637	15.2	0.4	-
190	ArchG125.60+04.18				$2.14 \pm 0.05$	$11.30 \pm 0.10$				-
191	ArchG125.91+03.22	$2.64 \pm 0.36$	$8.80 \pm 0.45$	1.55			01181+6541	4.8	0.4	-
192	ArchG126.37-01.31	$2.78 \pm 0.50$	$9.60 \pm 0.80$	0.79			01174+6110	30.7	33.9	-
193	ArchG126.40+00.33				$1.54 \pm 0.04$	$10.00 \pm 0.10$	01181+6251	11.5	1.3	LDN 1315
194	ArchG126.69-00.79				$4.00 \pm 0.02$	$18.60 \pm 0.10$	X0119+615	7980.0	5170.0	S 187 LDN 1317/
195	ArchG126.88-00.94				$1.54 \pm 0.02$	$9.90 \pm 0.10$	01214+6118	35.2	32.9	LDN 1324
196	ArchG127.34+03.60	$2.30 \pm 0.28$	$11.30 \pm 0.65$	0.94			X0131+657	50.6	53.4	-
197	ArchG127.69+02.65	$2.04 \pm 0.41$	$9.80 \pm 0.75$	2.91			01334+6442	6.4	0.5	-
198	ArchG127.74+01.19				$1.98 \pm 0.05$	$11.00 \pm 0.10$	01313+6322	21.6	1.9	-
199	ArchG128.28+05.87				$1.62 \pm 0.07$	$10.30 \pm 0.10$	01442+6749	5.4	1.1	-
200	ArchG128.60+04.19	$3.42 \pm 0.29$	$8.50 \pm 0.30$	1.75			01434+6609	18.6	0.4	-
201	ArchG128.93+04.35				$1.70 \pm 0.02$	$10.20 \pm 0.10$	01492+6608	11.4	0.4	-
202	ArchG129.22-00.24				$0.98 \pm 0.10$	$8.40 \pm 0.25$				LDN 1337, star cl
203	ArchG130.39-00.83	$2.52 \pm 0.38$	$10.70 \pm 0.75$	0.20			X0149+608	63.9	0.0	-
204	ArchG130.83-01.00	$2.24 \pm 0.36$	$10.10 \pm 0.70$	3.22			01527+6042	17.3	2.2	-
205	ArchG133.07+00.74				$1.86 \pm 0.03$	$10.70 \pm 0.10$	02148+6140	21.4	4.4	LDN 1354
206	ArchG133.24-00.04	$2.22 \pm 0.23$	$12.00 \pm 0.60$	3.45			02157+6053	215.0	21.8	-
207	ArchG133.42+00.08	$2.12 \pm 0.21$	$12.10 \pm 0.60$	2.32			02157+6053	215.0	21.8	-
208	ArchG133.69+01.21				$4.00 \pm 0.02$	$19.40 \pm 0.10$	02219+6152	42100.0	12000.0	W 3 LDN 1359 G
209	ArchG134.41+00.26				$3.10 \pm 0.03$	$14.00 \pm 0.10$	X0225+607	310.0	0.0	LDN 1363
210	ArchG134.64+02.29	$2.20 \pm 0.35$	$10.40 \pm 0.70$	0.32			02331+6225	26.6	3.0	-
211	ArchG135.09-00.07	$2.08 \pm 0.33$	$11.50 \pm 0.80$	1.63			02281+6010	80.6	10.9	LDN 1370
212	ArchG135.34+01.11				$2.56 \pm 0.02$	$12.40 \pm 0.10$	02338+6105	213.0	24.9	LDN 1372-1373
213	ArchG136.35+07.46				$2.24 \pm 0.04$	$11.60 \pm 0.10$	X0309+665	32.7	2.8	-

**Table 4.** continued.

N	Name	$\beta$	T (K)	$\chi^2_r$	$\beta_{11}$	$T_2$ (K)	Iras Name	$F_\nu(100\mu\text{m})/\text{Jy}$	$F_\nu(60\mu\text{m})/\text{Jy}$	Common Name A
214	ArchG136.58+01.11				1.88 ± 0.02	10.70 ± 0.10	02445+6042	60.0	41.1	-
215	ArchG136.85+01.07				2.44 ± 0.02	12.10 ± 0.10	02455+6034 *	340.0	168.0	W5 IR 1 HII G13
216	ArchG137.76+01.41	2.00 ± 0.12	14.60 ± 0.50	3.23			02531+6032	902.0	226.0	IRCO 3888
217	ArchG138.44+01.49				4.00 ± 0.02	17.80 ± 0.15	02589+6014	2100.0	1090.0	AFGL 4029 CLU
218	ArchG138.76+05.29				2.00 ± 0.02	11.00 ± 0.10	X0316+631	38.8	7.8	-
219	ArchG139.80+09.74				1.50 ± 0.05	9.90 ± 0.10	03492+6615	5.6	0.6	-
220	ArchG140.61+00.67	2.24 ± 0.40	11.80 ± 1.00	2.08			03107+5826	84.0	37.5	-
221	ArchG140.91-01.10				2.10 ± 0.02	11.20 ± 0.10	03057+5635 *	111.0	14.3	-
222	ArchG140.91+05.81	2.60 ± 0.30	8.80 ± 0.35	2.81			03353+6223	8.6	0.6	-
223	ArchG141.57-00.75				1.68 ± 0.02	10.30 ± 0.10	03099+5645	40.9	2.6	-
224	ArchG142.03+00.60	2.26 ± 0.24	11.40 ± 0.50	0.90			X0319+576	109.0	0.0	-
225	ArchG142.11+01.77				2.94 ± 0.02	13.50 ± 0.10	03233+5833 *	785.0	717.0	RAFGL 490 YSO
226	ArchG143.79-01.59	1.70 ± 0.28	19.10 ± 2.10	1.11			X0321+547	1860.0	1220.0	RAFGL 5094 HII
227	ArchG146.24-00.54	2.52 ± 0.38	10.60 ± 0.75	0.85			X0338+542	83.7	18.1	-
228	ArchG147.85+09.20	2.42 ± 0.33	10.20 ± 0.60	1.06			X0436+603	31.3	0.0	-
229	ArchG148.02+00.18	1.82 ± 0.20	13.10 ± 0.65	0.52			X0351+536	233.0	0.0	RAFGL 5107
230	ArchG148.43-00.68				2.38 ± 0.05	11.90 ± 0.10	X0349+528	62.9	0.0	-
231	ArchG148.79+02.18	3.12 ± 0.40	9.00 ± 0.50	2.34			04042+5444	40.1	4.0	-
232	ArchG150.41+03.91	3.20 ± 0.40	7.60 ± 0.35	0.29			04207+5445	6.1	0.4	-
233	ArchG150.63-00.87				3.98 ± 0.02	17.00 ± 0.10	X0359+511	2170.0	1180.0	S 206 RAFGL 51
234	ArchG151.49-00.36	1.14 ± 0.11	22.50 ± 1.25	1.70			04072+5100 *	2720.0	439.0	S 209 RAFGL 55
235	ArchG154.67+02.58	1.74 ± 0.14	16.30 ± 0.70	1.70			X0432+507	1190.0	635.0	S 211 RAFGL 51
236	ArchG157.06-02.82				1.88 ± 0.04	10.70 ± 0.10	X0420+452	27.3	5.2	-
237	ArchG158.00-21.44	1.30 ± 0.46	15.80 ± 2.50	3.82			03225+3034 *	169.0	25.1	-
238	ArchG158.34-20.53				2.92 ± 0.02	13.50 ± 0.10	X0326+312	1190.0	1080.0	RAFGL 5096
239	ArchG159.17-34.44	2.70 ± 0.25	8.50 ± 0.30	2.55			02530+1915	11.9	0.4	LDN 1457
240	ArchG159.17-20.11	2.22 ± 0.23	9.70 ± 0.35	4.03			03301+3057	35.5	6.2	-
241	ArchG159.23-20.38				1.18 ± 0.02	9.20 ± 0.10	03293+3052	10.9	1.4	-
242	ArchG159.75-19.41	2.26 ± 0.35	12.00 ± 0.90	1.39			X0334+312	200.0	0.0	-
243	ArchG160.21-18.45				2.12 ± 0.03	11.30 ± 0.10	03380+3143	79.7	3.7	-
244	ArchG160.37-18.12				1.62 ± 0.02	10.10 ± 0.10	03404+3156	56.7	4.5	LDN 1470
245	ArchG160.57-16.79	3.02 ± 0.38	8.30 ± 0.40	0.26			03445+3242	15.4	15.5	BARNARD 5 LDN
246	ArchG165.24-09.00	2.14 ± 0.10	18.50 ± 0.65	2.88			X0426+351B	10100.0	5800.0	S 222 RAFGL 58
247	ArchG168.10-16.35	2.98 ± 0.39	8.30 ± 0.45	3.81			04112+2803	15.8	3.0	-
248	ArchG168.79-15.63				2.32 ± 0.02	11.80 ± 0.10	04155+2812	168.0	72.7	RAFGL 5117
249	ArchG169.80-16.22	2.04 ± 0.54	9.90 ± 1.00	4.04			X0416+271	11.0	0.0	-
250	ArchG172.01-16.97				1.36 ± 0.04	9.50 ± 0.10	04204+2453	7.3	0.4	-
251	ArchG173.35+02.27	1.60 ± 0.14	14.40 ± 0.55	4.36			05351+3549 *	414.0	184.0	-
252	ArchG173.38-16.32	2.50 ± 0.16	9.60 ± 0.25	0.85			04263+2426	47.3	59.7	RAFGL 5122
253	ArchG173.52-01.75	1.86 ± 0.29	12.70 ± 0.90	3.50			05186+3326	147.0	23.0	S 236 G173.6-01.
254	ArchG173.62+02.77				2.98 ± 0.02	13.70 ± 0.10	05375+3540	1640.0	1710.0	S 235 G173.6+02
255	ArchG173.96-15.89	2.08 ± 0.35	9.40 ± 0.55	0.71			04292+2422	9.8	7.2	LDN 1529
256	ArchG174.05-13.79	2.96 ± 0.34	8.00 ± 0.25	4.54			X0437+256	11.7	0.0	LDN 1534 LDN 1
257	ArchG174.71-15.42				1.74 ± 0.03	10.40 ± 0.10	04325+2402	22.4	12.9	LDN 1535
258	ArchG175.24-12.27	3.16 ± 0.32	7.30 ± 0.25	1.86			04451+2542	2.6	0.4	-
259	ArchG175.61-16.76	2.98 ± 0.49	8.30 ± 0.55	0.36			04315+2232	9.7	0.7	-
260	ArchG176.61-01.76	1.82 ± 0.40	13.40 ± 1.45	0.26			05271+3059 *	166.0	94.9	-
261	ArchG177.50-20.29				1.60 ± 0.02	10.00 ± 0.10	X0424+187	16.0	0.0	-
262	ArchG178.85-20.09				2.88 ± 0.02	13.40 ± 0.10	04287+1801 *	458.0	373.0	RAFGL 5123 LDN
263	ArchG180.63-19.47				1.16 ± 0.14	8.70 ± 0.40				-
264	ArchG180.78+04.20				3.74 ± 0.03	16.20 ± 0.10	X0601+305	1450.0	719.0	S 241 RAFGL 51
265	ArchG182.02+00.36				1.68 ± 0.06	10.20 ± 0.10	X0548+273	13.7	4.0	-
266	ArchG182.09-00.50	2.54 ± 0.34	9.00 ± 0.50	2.93			05457+2649	12.8	1.1	-
267	ArchG182.17-17.89	1.84 ± 0.22	10.20 ± 0.40	3.15			04439+1651	9.9	0.4	-
268	ArchG182.44+00.25	1.40 ± 0.26	21.70 ± 2.70	1.93			X0548+270	1620.0	958.0	S 242 G182.4+00
269	ArchG183.21-00.65	1.36 ± 0.25	17.70 ± 1.70	0.76			X0548+257 *	481.0	133.0	-
270	ArchG183.63-03.74	2.30 ± 0.33	9.50 ± 0.50	4.80			X0536+238	13.4	3.8	-
271	ArchG184.55-05.77				1.78 ± 0.02	10.60 ± 0.10	X0531+219	202.0	165.0	CRAB W 09
272	ArchG184.58-04.14	3.06 ± 0.35	7.80 ± 0.35	2.26			05372+2253	4.6	0.5	-
273	ArchG185.56-02.39				1.06 ± 0.08	8.50 ± 0.20				-
274	ArchG186.43-05.43	2.04 ± 0.49	9.80 ± 0.90	4.03			05370+2027	6.4	0.4	-
275	ArchG186.76-05.35	1.68 ± 0.40	14.80 ± 1.80	1.85			X0538+203	195.0	62.8	-
276	ArchG188.43+02.96	2.08 ± 0.41	10.10 ± 0.75	0.27			06119+2303	12.2	0.7	-
277	ArchG188.51+03.59	1.90 ± 0.24	18.20 ± 1.50	1.93			X0615+233	1970.0	1040.0	LDN 1664 RAFGL
278	ArchG188.86+01.12				3.10 ± 0.02	14.10 ± 0.10	06061+2151 *	1130.0	896.0	RAFGL 5182
279	ArchG188.93+04.46				2.68 ± 0.03	12.70 ± 0.10	X0619+233	147.0	0.0	-
280	ArchG189.30+05.82				0.76 ± 0.02	8.50 ± 0.10	X0625+236	7.4	0.0	-
281	ArchG189.41-10.17				2.32 ± 0.05	11.80 ± 0.10	X0526+155	26.5	0.0	-
282	ArchG189.41+04.32				2.46 ± 0.02	12.20 ± 0.10	X0620+229	177.0	0.0	G189.4+04.4-HII
283	ArchG189.69+05.44				0.34 ± 0.08	7.00 ± 0.60				-
284	ArchG189.77+00.73	2.62 ± 0.26	10.00 ± 0.45	2.67			06067+2042	44.7	12.5	-
285	ArchG189.86+00.37				2.90 ± 0.02	13.50 ± 0.10	06055+2034 *	1720.0	73.0	NGC 2175 W 13
286	ArchG190.05+00.64				2.26 ± 0.02	11.70 ± 0.10	06068+2037 *	123.0	33.8	S 252 RAFGL 51
287	ArchG190.39-02.09				1.12 ± 0.08	8.60 ± 0.20				-
288	ArchG190.57+00.76				2.16 ± 0.02	11.40 ± 0.10	X0608+201	46.7	16.3	-

**Table 4.** continued.

N	Name	$\beta$	T (K)	$\chi^2_r$	$\beta_{11}$	$T_2$ (K)	Iras Name	$F_\nu(100\mu m)/Jy$	$F_\nu(60\mu m)/Jy$	Common Name A
289	ArchG191.64–00.84	$2.74 \pm 0.42$	$8.40 \pm 0.55$	4.57			06050+1824	5.1	0.5	-
290	ArchG191.86+00.88	$1.78 \pm 0.31$	$16.90 \pm 1.70$	1.15			X0611+190	673.0	368.0	-
291	ArchG192.04–02.72	$2.92 \pm 0.38$	$8.90 \pm 0.50$	2.72			05593+1711	13.1	4.8	-
292	ArchG192.24–03.87	$2.60 \pm 0.46$	$14.20 \pm 1.65$	0.35			05553+1631	528.0	421.0	RAFGL 5173
293	ArchG192.39–02.65	$3.84 \pm 0.40$	$7.30 \pm 0.30$	0.72			06000+1644	4.0	1.0	-
294	ArchG192.65–00.07				$4.00 \pm 0.02$	$19.10 \pm 0.10$	X0609+179	10700.0	7070.0	S 254 S 256 G192
295	ArchG192.65–03.78	$2.70 \pm 0.35$	$10.00 \pm 0.60$	4.87			X0556+161	33.7	6.7	-
296	ArchG193.96–02.54	$2.46 \pm 0.37$	$10.50 \pm 0.70$	0.34			X0603+154	23.8	0.0	-
297	ArchG194.01–00.43	$2.26 \pm 0.31$	$9.10 \pm 0.45$	1.62			06110+1632	5.4	5.0	-
298	ArchG194.41–00.92	$2.22 \pm 0.21$	$10.60 \pm 0.40$	0.36			06106+1608	26.0	0.8	-
299	ArchG194.73–03.49				$1.52 \pm 0.03$	$9.80 \pm 0.10$	06021+1431	11.4	2.9	-
300	ArchG194.83–01.17	$1.62 \pm 0.18$	$17.60 \pm 1.10$	2.56			06104+1524A *	444.0	252.0	RAFGL 5186
301	ArchG195.64–00.08	$2.04 \pm 0.16$	$15.10 \pm 0.65$	0.54			X0615+152B	565.0	348.0	RAFGL 5191 G195
302	ArchG195.73–02.39				$1.86 \pm 0.02$	$10.70 \pm 0.10$	06080+1410	26.2	5.8	-